GROUND MOTION UNCERTAINTY AND VARIABILITY IN EUROSEISTEST, GREECE

AUTHORS			REVIEW			APPROVAL		
NOM	DATE	VISA	NOM	DATE	VISA	NOM	DATE	VISA
Olga-Joan KTENIDOU ISTerre			Frank SCHERBAUM					
Zafeira ROUMELIOTI Univ. Thessaloniki			Philippe RENAULT					

***DISSEMINATION**: Authors; Steering Committee; Work Package leaders, Scientific Committee, Archiving.*

EDF Project 'Seismic Ground Motion Assessment' (SIGMA)
Contract no. 3000-5910108964

Ground motion uncertainty (sigma) and variability at EUROSEISTEST

SIGMA-2014-D2/D3-132
Joint Deliverable of WP2 & WP3

Olga-Joan Ktenidou, Zafeiria Roumelioti

Collaborators:
Norman Abrahamson, Facribe Cotton, Fabrice Hollender

14 October 2014

TABLE OF CONTENTS

EXECUTIVE SUMMARY 5
1. INTRODUCTION 7
1.1 Ground motion uncertainty and the single-station concept 7
1.2 The site under study 9
2. IMPROVING THE DATASET 14
2.1 Earthquake locations 14
2.1 Earthquake magnitude 14
3. STUDY OF GROUND MOTION UNCERTAINTY AND VARIABILITY 18
3.1 Improving global standard deviations and moving to single-station standard deviations 18
2.2 Single station standard deviations: stability, dependencies and site variability 23
2.3 Using existing GMPEs 30
4. COMPARING RECORDED AND SIMULATED VARIABILITY 42
5. CONCLUSIONS 43

EXECUTIVE SUMMARY

This report presents research conducted under Contract no. 3000-5910108964 and is submitted to EDF as Deliverable 3 under Article 3: 'Reunions - rapports'. It also contains research

Chapter 1 makes an introduction to the topic of ground motion uncertainty and the single station concept within a PSHA framework, and then presents the site under study, our dataset. Our goal is to study ground motion variability in as well constrained a dataset as one may be expected to find today, in terms of records, source parameters, and site information.

Chapter 2 presents the procedure by which our dataset's source parameters (event location and magnitudes) were optimised after a series of catalogue researches and correlations, event relocations, and spectral analyses. This is of critical importance to this study because it will reduce the global uncertainties, namely the between-event component, as much as possible and allow analysis of within-event residuals in the single-station concept.

Chapter 3 includes the main part of the analysis, where we create a simple GMPE to remove the mean from our data and analyse residuals. We first investigate how we can decrease the components of global aleatory uncertainty by improving our source and site data. The importance of the previous step is demonstrated through the large decrease achieved on τ. The importance of having good site knowledge is then shown in the decrease on $\varphi s2s$ and φ. Then we pass on to single-station components of uncertainty. We compare our values to results found across literature and find them to be lower. We examine the behaviour of uncertainty components with period from 0.01 to 2 s and the sensitivity to the number of records used. Despite some correlations in the data, a criterion of 3 records per event is sufficient. We identify the stations of the array with the highest and lowest site variability (φss) and point out some effects of the GMPE formulation (namely, its site response predictor variable) to the systematic deviation $\delta s2s$. By binning our data with respect to magnitude, distance and depth, we observe tendencies at different periods, some of which are in agreement with observations made on global datasets with higher magnitudes. We look at the closeness index and discuss possible effects of the azimuthal coverage of source-site paths around the site. Finally, we investigate an alternative approach towards computing φss: the use of existing predictive GMPEs in lieu of creating an ad hoc GMPE with local data. We select some models from Greece and Europe calibrated for larger magnitudes. We find that the φss component can also be computed this way, under the conditions that the magnitude scaling errors are picked up by the event terms, and there is no error in distance scaling. This implies the need to use a regionally applicable model.

Chapter 4 is a placeholder referring to Chapter 6 in the WP3 deliverable SIGMA-2014-D3-137 ('3D ground motion simulations for site effects assessment: learnings from EuroseisTest Verification and Validation Project'), not available at the time of submission of this document. The chapter shows preliminary comparisons of ground motion variability between this dataset and the simulations carried out under WP3.

Chapter 5 summarises the work and describes topics that need further research.

The Annex contains a list of publications made during this contract, relevant to the topic of uncertainty in ground motion prediction.

1. INTRODUCTION

1.1 Ground motion uncertainty and the single-station concept

Probabilistic Seismic Hazard Assessment (PSHA) has often been shown to be strongly influenced by the uncertainty in strong ground motion estimation, especially at long return periods, i.e., low annual rates of exceedance (e.g. Bommer and Abrahamson, 2006). Ground motion prediction is primarily done through the use of empirical relations usually called Ground Motion Prediction Equations (GMPEs) and its variability, commonly referred to as **sigma (σ)**, is broadly interpreted as aleatory variability, i.e., scatter attributed to the random and complicated nature of the physical processes of the generation and propagation of seismic waves in the earth's interior. However, several studies (e.g. Anderson and Brune, 1999) have suggested that such an interpretation is not accurate and that a fraction of sigma should be treated as epistemic uncertainty, i.e. uncertainty that can be resolved with the appropriate amount of knowledge and data. According to Anderson and Brune (1999), this is because part of the variability in ground motion is due to path and site effects, which may be repeated in subsequent earthquakes. Identifying and quantifying this epistemic fraction could optimally lead to a decrease in sigma and hence to more realistic PSHA results. This is of primary importance when designing ground motion for critical facilities such as nuclear power plants and related infrastructure.

Accepting an epistemic fraction of sigma means dropping the **ergodic assumption** (Anderson and Brune, 1999). In the ergodic approach, we compensate for the lack of data in time with data in space, and the spatial and temporal variability of ground motion are considered equal. Hence, the expected variability of strong ground motion at a specific site is assumed to be equal to the sigma of the GMPE that is adopted for that site. However, GMPEs are rarely constrained by data from a specific site, fault, or even region, but are usually constructed on the basis of more global sets of data from regions of similar (or not so similar) seismotectonic characteristics. In fact, as strong ground motion data have rapidly increased during the past decades, it has been made possible to test the hypothesis of ergodicity and it appears that variability of strong ground motion at a specific site, commonly referred to as **single-station sigma** is usually much lower that the variability of global GMPEs (e.g. Chen and Tsai, 2002; Atkinson, 2006; Morikawa et al., 2008; Rodriguez-Marek et al., 2011, 2013). The same conclusion applies to a certain source-station path, repetition of which may lead to even lower variability (Lin et al., 2011).

In the quest of sigma components, Joyner and Boore (1981) were the first to separate the aleatory variability into inter- and intra-event variability. Nowadays, most scientists seem to adopt the corresponding terms of "between-event" and "within-event" variability suggested by Al. Atik et al. (2010), which are illustrated by Strasser et al. (2009) in Figure 1.1. The notation of Al Atik et al. (2010) is used throughout this deliverable. Between-event variability is observed on events of the same magnitude and style-of-faulting and is attributed to differences in the source rupture process such as different stress-drop, rupture velocity, slip velocity, etc. Within-event variability is practically the spatial variability observed during a specific event between sites at the same distance from the source. This latter component of sigma is attributed to phenomena pertinent to the deep geological structure and the geotechnical characteristics of the sites, such as ground motion amplification, near-surface attenuation, propagation effects and nonlinear site response. The between- and within-event residuals are generally assumed to be uncorrelated and thus the total standard deviation is computed as the square root of the sum of the squares of the between- and within-event standard deviation, commonly referred to as tau (τ) and phi (φ), respectively.

τ and φ are the standard deviations of the between-event and within-event residuals (δB_e and δW_{es}, respectively with subscripts denoting an observation for an event *e* and a station *s*, which added form the total residuals (Δ_{es}) of a GMPE:

$$\Delta_{es} = \delta B_e + \delta W_{es} \quad (1.1)$$

The within-event residuals can be broken down to:

$$\delta W_{es} = \delta S2S_s + \delta WS_{es} \quad (1.2)$$

where given multiple recordings of ground motion at a specific site *s*, $\delta S2S_s$ is the systematic deviation of the observed amplification at this site from the empirically predicted median amplification that could be attributed, for example, to site effects. Then, δWS_{es} is the remaining within-event residual at site *s* from event *e*, i.e, the part of the residual that does not appear in a systematic manner. The standard deviations of $\delta S2S_s$ and δWS_{es} are denoted by φ_{S2S} and φ_{SS}, respectively. This latter term, φ_{SS}, is what is commonly referred to as **single-station phi** and is used to compute the **single-station sigma (σ_{SS})**, i.e. the aleatory variability of the ground motion model at a single site under the partially non-ergodic assumption. The standard deviations of equation (1.2) and the single-station sigma constitute the parameters to be primarily investigated in the present deliverable. It is important to note that partially (single-station) or fully (single-path) non-ergodic sigmas should not generally be used unless there is sufficient data to estimate -either empirically, theoretically, or numerically- the site response. This is because φ_{S2S} can only be dropped from the aleatory uncertainty of the global GMPE if the error of the site response calculations is added to the epistemic part of the uncertainty within the PSHA framework. Furthermore, this causes the mean of the global GMPE to change, so that the non-ergodic sigmas should be used with an ad-hoc, site- or path-specific GMPE.

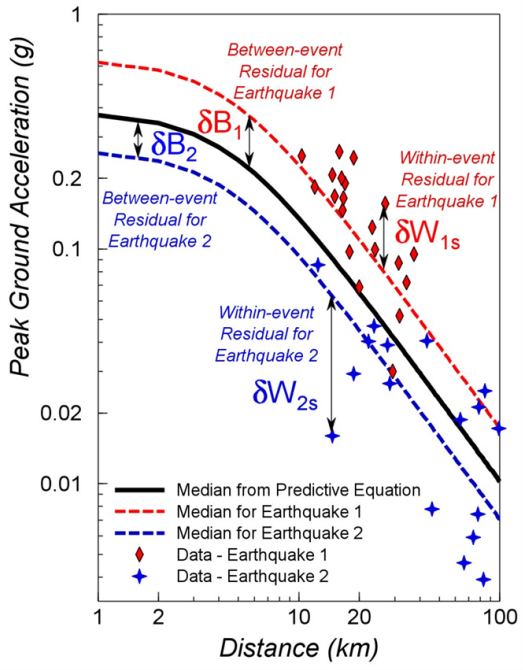

Figure 1.1. Schematic representation of within-event and between-event residuals (after Strasser et al., 2009).

1.2 The site under study

We choose to study a small region and work with a dataset that is as well constrained as possible with respect to what is encountered in practice, in order to be able to better constrain epistemic uncertainty and investigate the contribution of different parameters on the global and single-station aleatory uncertainty. For this purpose we choose a specific site, the EUROSEISTEST valley (Pitilakis et al., 2013; http://euroseisdb.civil.auth.gr), where metadata are well constrained, the seismotectonic environment well studied, and data are reasonably homogeneous.

The most distinct advantage of our dataset is the good existing knowledge of site conditions, which is a result of more than 20 years of geophysical, geotechnical, and site response studies in EUROSEISTEST (e.g., Jongmans et al., 1998; Raptakis et al., 1998, 2000; Kudo et al., 2002; Manakou et al., 2010). The key to using lower σ values in site-specific GMPEs is being able to achieve a reliable site-specific site/path term. This knowledge makes it possible to test our analysis for different levels of site information, starting from crude soil vs. rock descriptions, and moving to a more elaborate site description based on Vs_{30}. This is shown to be important in the results of the study.

EUROSEISTEST is a geologically complex and seismically active region with a permanent strong motion array consisting of 14 surface and 6 downhole stations (Figure 1.2). The depth of the deepest downhole station is almost 200 m, and the span of the valley is about 5.3 km. Site conditions range from soft sediments to hard rock, with Vs30 from 190 to 1840 m/s (site classes spanning from A to C/D, according to EC8). Most stations are located on soil, so –as is most often the case– the dataset cannot be said to represent equal amounts of soil and rock data. The coexistence of such different site types, including hard rock, is nevertheless a significant advantage.

Another advantage of this dataset is that it can be well controlled in terms of the quality of its metadata, as it refers to a relatively small, well-studied area and to events after 2003, i.e., after the modernisation and densification of permanent monitoring networks in Greece. Metadata is of fundamental importance in our study, as we are dealing with small distances from the source and small magnitude events (Figure 1.3). All events in our dataset have been carefully relocated and magnitudes re-estimated with respect to routine parameters retrieved from monthly seismic bulletins. Hence, we can also test our analysis for different levels of source information, i.e. for the typical catalogue quality and for expert relocation quality.

We create an initial database based on quality criteria, including 814 records from 133 events, with moment magnitudes from M1.5-M6.5 and distances from 1-400 km. For the purpose of this study we refine the dataset as follows. We do not include events at distances longer than 225 km, or records that do not have both horizontal components. We reject events which may come from a subduction regime, thus we keep focal depths to a maximum of 16 km. Most importantly, given the nature of this study, we must reject all events that were not recorded by at least 3 stations, because these may lead to inadequate resolution of the event terms and hence inflated values of τ. Our final dataset consists of 691 records from 74 events, with magnitudes from M2.0-M5.6 and distances from 5-220 km (Figure 1.3). The geographical distribution of earthquake epicentres in the final data set is presented in Figure 1.4. In Figure 1.5, we present the number of records per event for our initial data set of 133 events and the records not used in subsequent analysis

due to the fact that they had been recorded by only one or two stations.

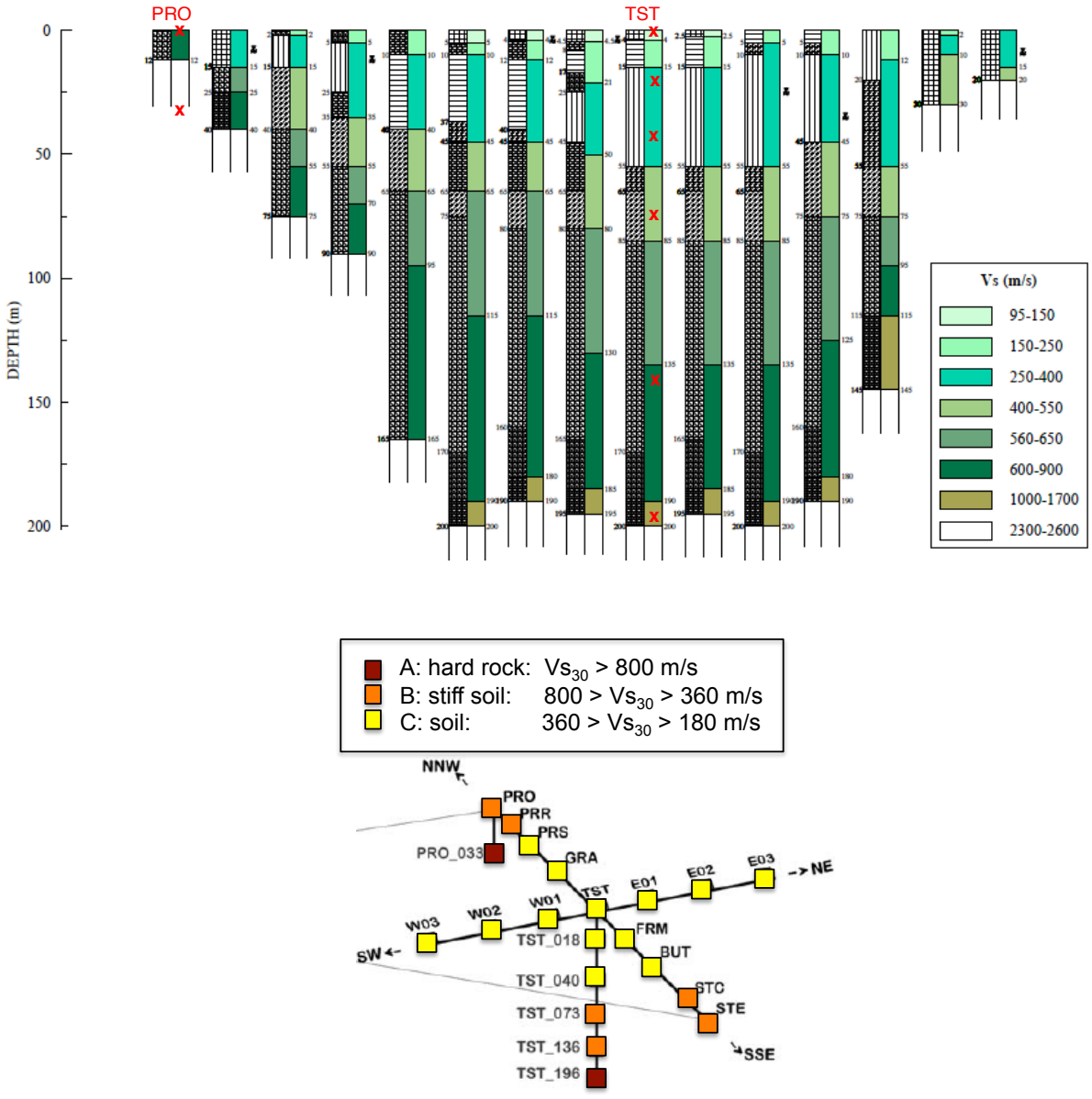

Figure 1.2. Top: Indicative geotechnical section and Vs profiles, including location of surface stations and downhole instruments in the two boreholes. Bottom: 3D sketch of the array, with a colour code indicating EC8 classification (adapted from Pitilakis et al., 1999 & 2013).

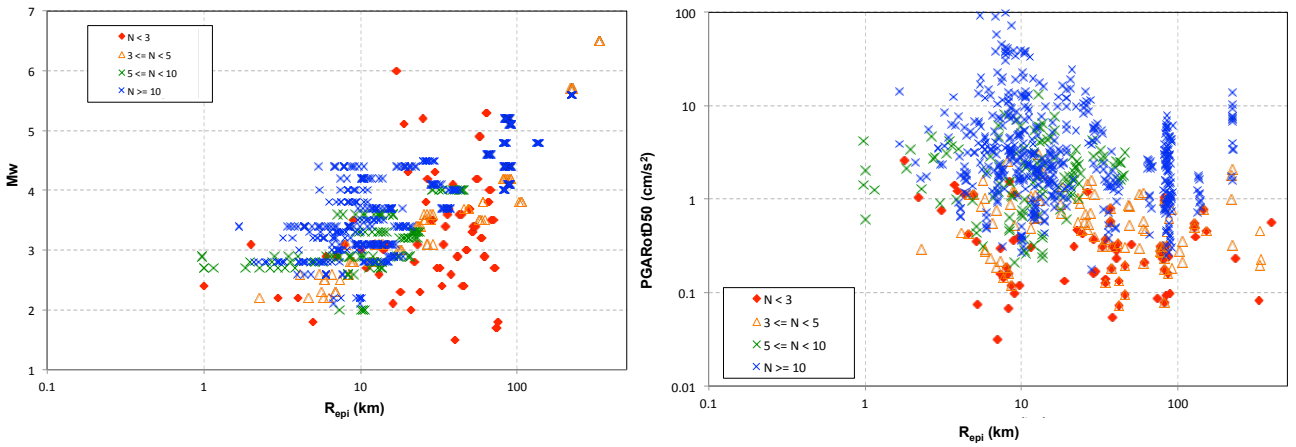

Figure 1.3. Magnitude and epicentral distance distribution (left) and PGA values for the RotD50 average horizontal component with distance (right), colour-coded to show the data available according to the number of records per event.

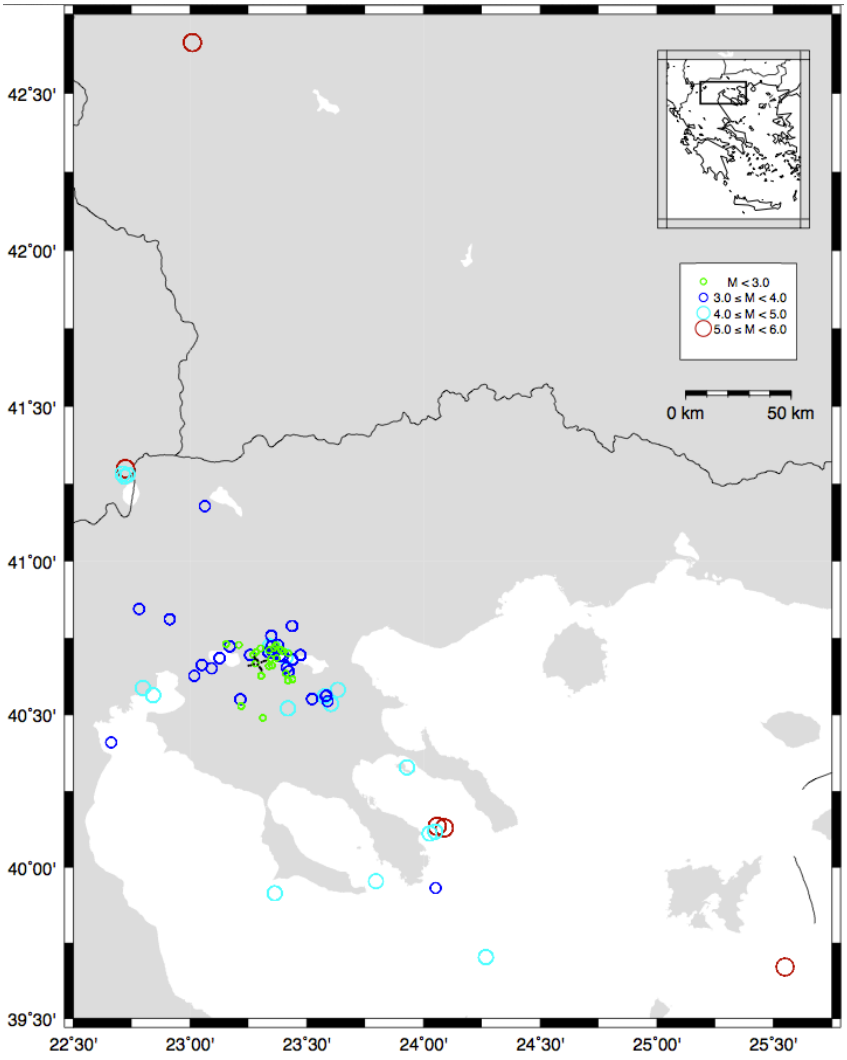

Figure 1.4. Epicentral distribution of the dataset, colour-coded with magnitude. The cross indicates the location of the array. (This map does not show events farther than 250 km, which were rejected).

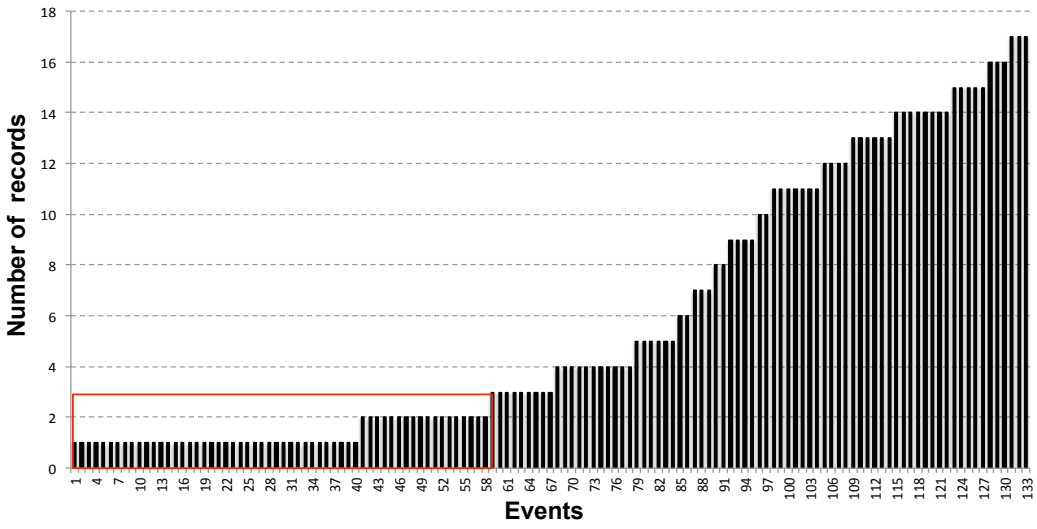

Figure 1.5. Number of records per event in the dataset (red zone indicates data that cannot be used).

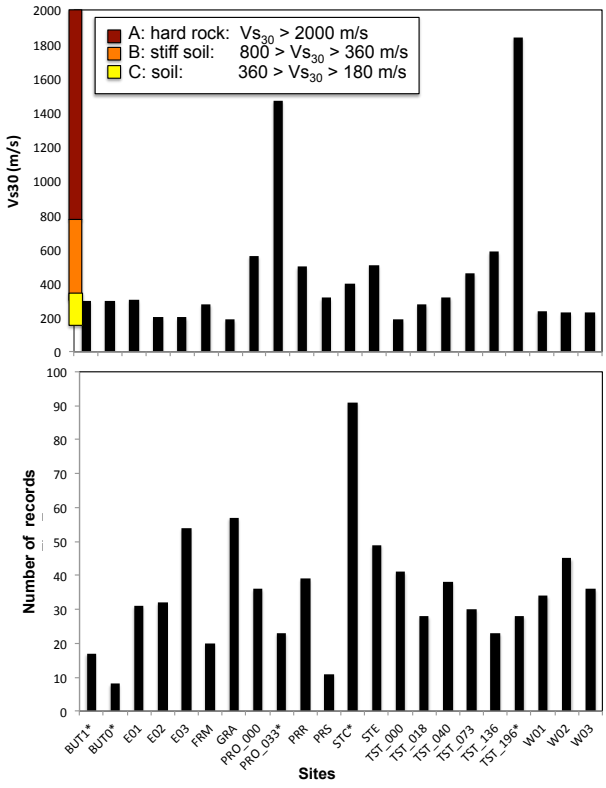

Figure 1.6. Number of records and Vs30 per station.

In Figure 1.6 we show the distribution of examined records per station (bottom) and the V_{S30} value that we assigned to each recording site after having examined all the available geological, geotechnical and

geophysical information provided in the EUROSEISTEST web portal (http://euroseisdb.civil.auth.gr). The distribution of records at the EUROSEISTEST stations is relatively uniform, whereas most recording sites are characterized as soft soil sites. In general, there is a satisfactory diversity in soil categories ranging from quite soft soils at the centre of the valley (e.g. stations TST_000, GRA, FRM) to hard rock at the edges (station PRO_033) and at the deepest downhole station (TST_196).

Accelerometric data used in our analysis correspond to the 'filtered' data set of the EUROSEISTEST database (Pitilakis et al., 2013). These data have been filtered using an acausal, 4th-order band-pass Butterworth filter and a threshold value of 3 for the signal-plus-noise to noise ratio. The distribution of lowest and highest usable frequencies in the records of the dataset is shown in Figure 1.7. As can be concluded from this Figure, corner frequencies and especially the low-cut corners vary significantly among the different records and this should be kept in mind when single station analysis results are interpreted at discrete periods.

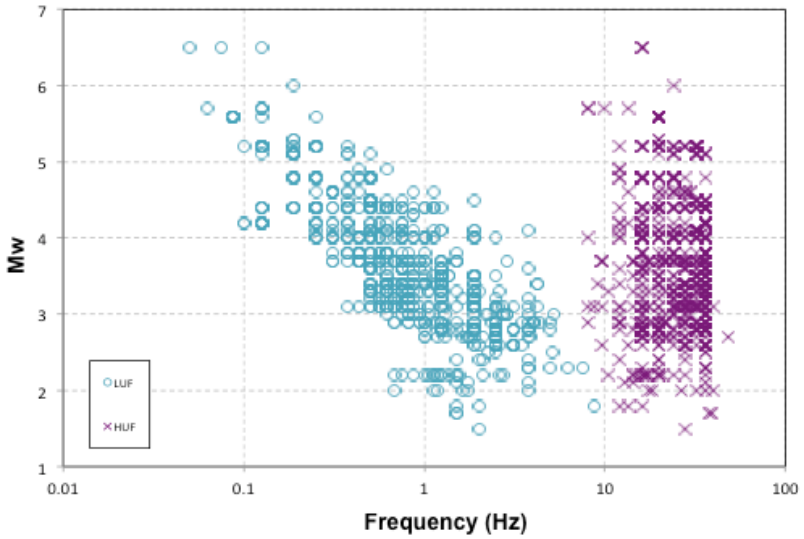

Figure 1.7. Lowest and highest usable frequencies for each record in the dataset. The magnitude dependence of LUF means that we will have fewer data to work with at longer periods.

2. IMPROVING THE DATASET

It is well known that errors in the predictor variables can contribute significantly to the standard deviation of a distribution through error propagation. It is, thus, of primary importance to reach the maximum possible accuracy for all independent variables included in our dataset, and more specifically, for earthquake locations (determining the distance variables) and earthquake magnitude.

To investigate the effect of metadata accuracy in our single station analysis, we processed two flatfiles: the first one containing routine earthquake locations and magnitude determinations, and the second one with relocated earthquake foci and revisited moment magnitudes. The differences between the two flatfiles are described in more detail in the following.

2.1 Earthquake locations

Routine earthquake location determinations for the broader EUROSEISTEST area are provided by the Institute of Geodynamics of the National Observatory of Athens (NOA, http://www.gein.noa.gr) and the Department of Geophysics of the Aristotle University of Thessaloniki (THE, http://seismology.geo.auth.gr). Until 2008, the two Institutes were using different data sets, with THE having more stations around our study region. Since 2008, NOA, THE, and the University of Patras (http://seismo.geology.upatras.gr) combined their permanent seismological networks to form the Hellenic Uniform Seismological Network (HUSN). Since then, all HUSN partners share the same dataset, although phase picking and routine earthquake location on a 24/7 basis is performed independently by both NOA and THE.

Although routine earthquake locations in EUROSEISTEST are expected to be quite accurate due to the dense and sufficient azimuthal coverage of the area by the permanent seismological stations, a relocation of the recorded seismicity is expected to reduce by a considerable amount the epistemic uncertainty in single station computations, especially through the improved determination of focal depths. Events that occurred before the establishment of HUSN may be less accurately located compared to events that occurred after 2008.

For our starting flatfile, we chose to use the solutions of THE, as its network, prior to the HUSN establishment, had been denser around the EUROSEISTEST location. However, for a quite large period of time (up to December 2005) THE data have been reprocessed and events have been relocated by Galanis (2010). These relocated solutions substituted the routine determinations in our second, more refined flatfile. For those events that occurred after December 2005, we adopted the solutions of THE and only re-processed those events with epicentres at distances up to 30 km from the centre of the EUROSEISTEST array by adding P- and S-wave arrivals picked on the strong ground motion recordings at the rock stations of EUROSEISTEST (PRO_033, STE and TST_196). Locations were re-determined using the same algorithm (HYPOINVERSE; Klein, 2002) and velocity model (Panagiotopoulos, 1984) used in THE routine analysis, which have been shown to work well for the broader study region.

2.1 Earthquake magnitude

Perhaps the most uncertain information in our metadata set is related to earthquake magnitude, especially for those events that occurred before the year 2008, i.e., before the establishment of the HUSN. This is because most of the events in our dataset are of small magnitude, and in many cases M_w had to be inferred by published M_L. On the other hand, NOA and THE had been using different approaches to compute M_L before the establishment of HUSN and furthermore the comparison between M_L and M_w has not been consistent throughout the years due to alterations in the monitoring networks or/and the M_L measuring practices (Roumelioti et al., 2011). Revisiting earthquake magnitude values is of primary importance, since the magnitude variable has been shown to greatly influence the variability during the regression analysis, especially the inter-event variability (e.g. Rhoades, 1997; Klügel et al., 2006).

For our starting flatfile, we used the magnitude values published in the monthly seismicity bulletins of THE (http://geophysics.auth.gr/ss). However, in our refined flatfile, we collected magnitude determinations from different sources and made judgements on the most appropriate value to be assigned to each one of the events. More specifically, we collected magnitude values published in THE and NOA seismicity bulletins (denoted $M_{L(AUTH)}$ and $M_{L(NOA)}$ respectively in Table 1). Both these sets of values were empirically corrected following the suggestions of Roumelioti et al. (2011), to retain equivalence of the M_L with the M_W computed by the two institutes throughout the examined time period. Thus, we derived two new sets of magnitude values, referred to as $M_{L(AUTH)cor}$ and $M_{L(NOA)cor}$ (also in Table 1), which are equivalent to M_W. For small magnitude earthquakes that could not have been recorded by the Wood-Anderson seismograph operating in NOA (see Roumelioti et al., 2011 for more details on magnitude estimation procedures in NOA), no M_L estimation was available in the seismicity bulletins of the Institute. However, there was usually a duration magnitude (M_D) estimation available, which has been calibrated against M_L published by NOA and is considered equivalent to the latter and, thus, to M_W. We added these values in a separate column ($M_{D(NOA)}$) in Table 1 for the sake of clarity. Another independent estimation of the magnitude for most of the events in our data set came from the unpublished work of S. Drouet (personal communication) using the joint inversion methodology described in Drouet et al. (2008). These values are presented in the column named $M_{(INV)}$ in Table 1. We also gathered all published M_W values for events in our dataset, mostly coming from moment tensor inversions ($M_{W(MT)}$). References to sources of M_w values for individual events can be found on the EUROSEISTEST web portal (http://euroseisdb.civil.auth.gr). Finally, wherever possible, we performed our own re-assessment of M_W through spectral analysis of the strong motion records at rock stations of EUROSEISEST (PRO_033, STE, TST_196). The mean M_W for each event, $M_{W(SA)}$, is also presented in Table 1.

Based on the aforementioned independent estimations of the earthquake magnitude of each event in our dataset, all equivalent to M_W, we made judgements as to the most appropriate value, which is shown in column M_W of Table 1. These latter values are the ones used in our subsequent analysis.

Table 2.1. Different magnitude values associated to each event in our database. M_W: magnitude adopted in our analysis, $M_{L(AUTH)}$: local magnitude in AUTH seismicity bulletins (http://seismology.geo.auth.gr/ss), $M_{L(AUTH)cor}$: as previous, but corrected after Roumelioti et al. (2011), $M_{L(NOA)}$: local magnitude from NOA seismicity bulletins (http://www.gein.noa.gr), $M_{L(NOA)cor}$: as previous, but corrected after Roumelioti et al. (2011), $M_{D(NOA)}$: duration magnitude reported in NOA bulletins, $M_{(INV)}$: moment magnitude from joint inversion (Drouet et al., 2008), $M_{W(MT)}$: moment magnitude from moment tensor inversion, $M_{W(SA)}$: moment magnitude from spectral analysis.

Event	M_w	$M_{L(AUTH)}$	$M_{L(AUTH)cor}$	$M_{L(NOA)}$	$M_{L(NOA)cor}$	$M_{d(NOA)}$	$M_{(INV)}$	$M_{w(MT)}$	$M_{w(SA)}$
2004-03-27 10:39	**4.0**	4.1	4.2	3.8	4.0		3.99		4.0
2004-06-04 18:19	**3.0**	2.9	3.0			3.0	3.15		3.16
2004-06-08 22:38	**3.3**	3.4	3.5			3.3	3.33	-	3.3
2004-07-15 00:40	**3.7**	3.5	3.6			3.7	3.55	3.94	3.7
2004-07-15 04:12	**3.7**	3.5	3.6			3.7	3.46	3.8	3.7
2004-11-09 11:46	**3.1**	2.9	3.0	-	-	3.1	3.11	-	3.1
2004-11-19 21:01	**2.9**	2.8	2.9	-	-	3.1	3.04	-	2.9
2004-12-12 23:32	**2.7**	2.6	2.7	-	-	3.0	2.64	-	2.75
2005-01-30 20:33	**2.6**	2.5	2.6				2.55		2.49
2005-04-20 07:52	**3.7**	3.7	3.8	4.1			3.52	3.8	3.5
2005-09-12 19:08	**4.4**	4.3	4.4	4.3	4.5	-	4.34	-	4.5
2005-09-12 19:16	**2.5**	2.2	2.3	2.8					2.52
2005-09-12 19:26	**4.0**	3.9	4.0	4.0			3.69		4.09
2005-09-12 19:52	**3.0**	2.9	3.0			3.2	2.95	3.2	3.0
2005-09-20 17:41	**3.2**	3.1	3.2	-	-	3.3	3.32	-	3.2
2005-10-09 07:12	**3.8**	3.9	4.0	-	-	3.6	3.82	-	3.75
2005-10-09 11:12	**3.4**	3.5	3.6			3.4	3.33	-	3.4
2005-10-09 12:30	**3.3**	3.4	3.5	-	-	3.3	3.32	-	3.2
2006-01-13 21:36	**3.5**	3.4				3.6			3.50
2006-02-11 19:01	**2.8**	2.8				3.3			2.72
2006-03-02 04:52	**3.8**	3.8		3.7					4.11
2006-04-13 04:36	**2.9**	2.3				3.2			3.34
2006-05-10 07:01	**4.4**	4.3	-	4.0	4.2		4.43	4.4	4.6
2006-08-17 04:27	**3.6**	3.6	-	3.9	4.1	-	3.60	-	3.54
2007-04-19 10:15	**4.8**	5.4		4.8				4.6	4.79
2007-05-29 02:29	**2.9**	3.2	2.8			3.4			3.06
2007-07-18 19:09	**4.0**	4.7	4.3	4.0				4.0	4.0
2007-11-02 14:50	**3.1**	3.8	3.4			3.5			3.1
2007-11-03 01:00	**3.3**	3.7	3.3			3.5	3.28		3.2
2007-12-27 16:55	**3.5**	3.9	3.5	-	-	3.4	3.36	-	3.5
2008-01-05 05:30	**3.2**	3.4	-	-	-	3.3	3.27	-	3.0
2008-08-28 09:31	**2.8**	2.7	-			3.0	2.97	2.8	2.8
2008-08-29 04:49	**2.6**	2.1				2.9	2.60		2.68
2008-09-05 21:32	**3.4**	3.5		3.8			3.37		3.36
2008-10-13 07:26	**2.8**	2.8	2.8				-	-	2.9
2008-11-28 00:38	**2.3**	1.9				3.2	2.59		2.27
2008-11-29 03:23	**2.6**	2.3				3.0	2.62		2.77
2008-12-27 08:27	**4.4**	4.4		4.1			3.98	4.1	4.35
2008-12-27 20:09	**4.1**	4.5		4.3			4.23	4.1	4.1
2009-01-13 11:57	**4.2**	4.4		4.0			4.15		4.34
2009-05-24 14:29	**4.2**	4.2		3.8				4.1	4.3
2009-05-24 16:17	**5.2**	5.0		5.1			4.73	5.2	5.4
2009-05-24 16:23	**4.4**	4.4		4.2				4.4	4.4
2009-05-24 19:37	**4.8**	4.8		4.5				4.5	4.8
2009-06-21 22:48	**3.1**	3.4	-	3.0	-	-	3.21	-	3.0
2009-10-15 14:47	**3.4**	3.1	3.1			3.4	-	-	3.4
2010-02-09 14:16	**2.8**	2.8				2.9			
2010-04-05 12:25	**2.8**	2.4				3.1			
2010-05-31 19:27	**2.7**	2.5				3.0			
2010-08-08 09:00	**4.5**	4.5		4.5			-	4.4	4.6
2010-08-08 09:14	**4.1**	4.4		4.3				4.4	

2010-08-08 09:59	**3.6**	3.6		3.5				3.6
2010-09-06 08:25	**3.1**	3.0			3.0			3.19
2010-11-29 16:03	**3.5**	3.6		3.5			3.5	3.70
2011-01-03 04:13	**2.8**	2.4			2.8			2.76
2011-01-14 19:25	**3.6**	3.2		3.0				3.64
2011-02-09 19:59	**2.9**	2.2		2.1				2.89
2011-07-25 04:25	**2.8**	2.5		2.4		-	2.8	2.9
2011-08-07 09:15	**4.0**	4.1		3.9			3.9	4.05
2012-02-14 01:34	**5.1**	5.0		5.0			5.1	5.52
2012-03-04 03:31	**5.2**	5.0		5.0			5.2	5.66
2012-05-12 22:48	**4.0**	4.0		4.1			4.0	4.05
2012-05-22 00:00	**5.6**						5.6	
2012-07-24 01:53	**2.9**	2.4						2.9
2012-10-21 04:43	**3.4**	3.3	3.3	3.3		-	3.44	3.5
2013-01-08 14:16	**5.7**	5.9		5.8			5.7	5.79
2013-02-15 14:42	**4.6**	4.7		4.6			4.5	4.6
2013-05-03 16:22	**3.8**	3.8		3.7				3.97
2013-09-09 02:17	**3.7**	3.3		3.3				3.77
2013-10-11 05:15	**4.2**	4.4		4.4			4.2	4.25
2013-10-11 05:57	**2.2**	2.2		2.2				2.25
2013-10-11 06:14	**2.0**	2.0		2.0				2.05
2013-10-11 06:18	**3.1**	3.0		3.1				3.15
2013-10-11 06:41	**2.1**	2.1		2.1				2.0
2013-10-11 09:18	**2.2**	2.3		2.2				2.15

3. STUDY OF GROUND MOTION UNCERTAINTY AND VARIABILITY

3.1 Improving global standard deviations and moving to single-station standard deviations

We first wish to investigate how we can decrease the components of global aleatory uncertainty by improving our source and site data. As explained in Chapter 1, we have narrowed down our dataset to crustal events, distances less than 225 km, and records that have both horizontal components. This leaves us with events whose magnitudes do not exceed M5.7, which means that they can be regarded roughly as point sources. Hence, we consider that rupture distance (Rrup) can be approximated by hypocentral distance (Rhyp) and Joyner-Boore distance (Rjb) can be approximated by epicentral distance (Repi). We have further decreased the dataset to include only events that were recorded by at least 3 stations, so as to correctly estimate the event term. Given the small number of stations in the array (22) and the large number of events each station recorded, we are confident that the site term can be estimated well. We have computed the PGA and spectral acceleration (SA) at various periods from 100 Hz up to 2 s.

We create a simple GMPE from our data, using a formula including magnitude, distance (Rrup, i.e. Rhyp), and a site parameter which varies. The goal of this model is not to be used outside this study for prediction purposes, but to capture the mean of our data and allow us to compute well-balanced residuals for the purpose of studying standard deviation. We regress our data using a mixed (fixed and random) effects model after Abrahamson and Youngs (1992). The total aleatory uncertainty of ground motion, σ, is the standard deviation of the total residuals between our data and the model's predictions We break up these residuals into between-event (δBe, Figure 3.1) and within-event (δWes, Figure 3.2a, top), where e stands for event and s stands for station, and compute their standard deviations, τ and φ. These are the standard deviations typically considered in an ergodic framework, as explained in Chapter 1. As seen in Figure 3.1, δBe are not correlated with magnitude, thus verifying that the magnitude scaling of our GMPE describes the centre of our data well. For each station, we compute the mean of the δWes and thus estimate the systematic, site-specific terms (δs2s), whose standard deviation gives us φs2s. Correcting each station's δWes with the site term, δs2s, we then have the site-corrected within-event residuals, or δWSes. Figure 3.2a shows that these are not correlated to distance, indicating that the distance scaling in our GMPE describes the centre of the data well. The standard deviation of each station's δWSes gives us that site's single-station variability, or φss,s (Figure 3.2b). We verify that φss,s and ds2s,s are not correlated to Vs30 or the number of events each station recorded (Figure 3.2b).

Single-station standard deviations are typically considered only when the traditional ergodic framework is abandoned in favour of site-specific analyses, as was explained in Chapter 1. In such a case, the total ergodic σ and the φ can be reduced by removing the ergodic assumption, and using instead σss and φss. This would be possible in this site thanks to the good knowledge of site conditions and the available recorded data that allow us to compute site response both theoretically and empirically. In this case, we stress that the global median of the GMPE can no longer be used and a new, site-specific one, should be estimated.

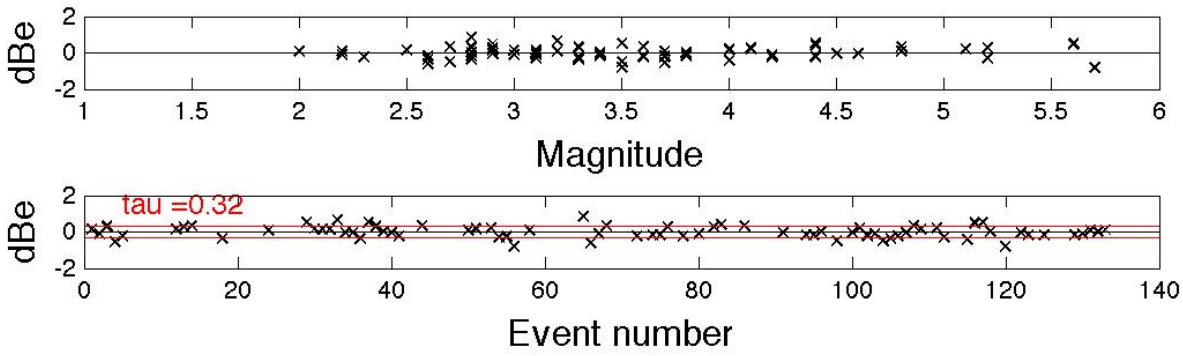

Figure 3.1. Example of the correlation of between-event residuals (dBe) with magnitude (top) and the estimation of τ (bottom). These results are at PGA, for the relocated dataset, using a GMPE with quadratic scaling and Vs30 as a site proxy.

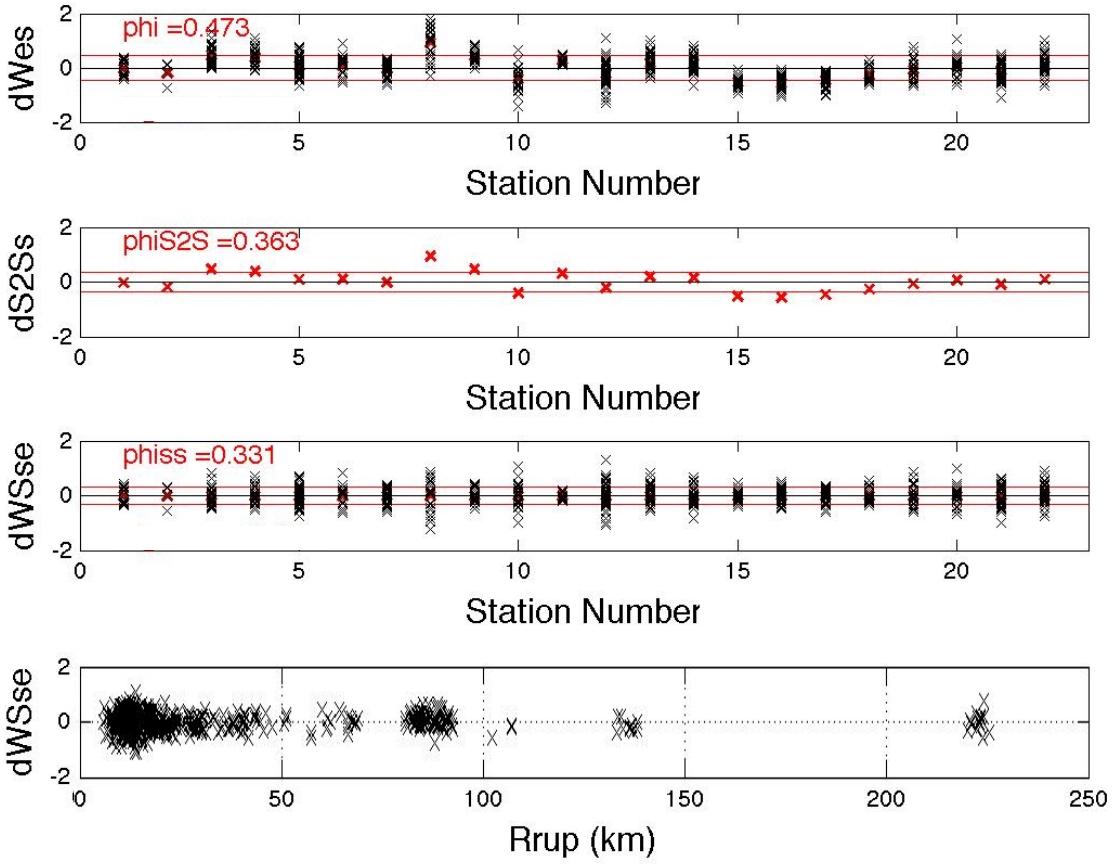

Figure 3.2a. Example of the break-up of within-event residuals (dWes, top) into the systematic site term (ds2s, upper middle) and site-corrected within-event residuals (dWSes, lower middle), and of the estimation of φ, φs2s, and φss respectively. Bottom panel shows the correlation of dWSes with distance. These results are at PGA, for the relocated dataset, using a GMPE with quadratic scaling and Vs30 as a site proxy.

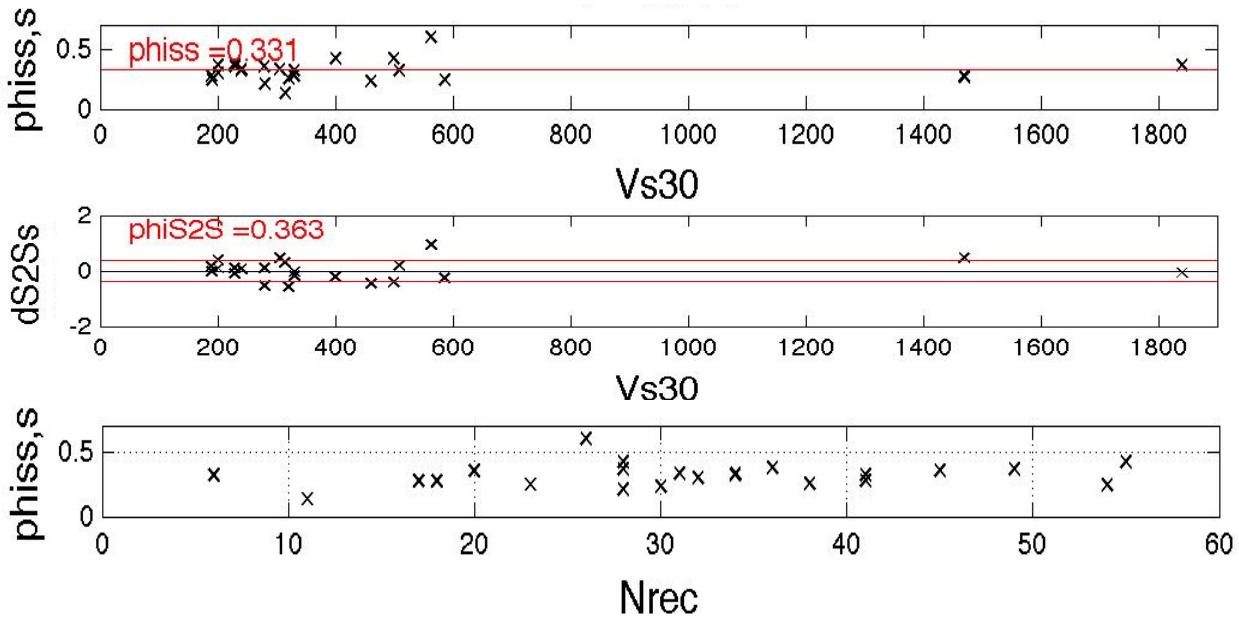

Figure 3.2b. Example of the correlation of δs2s,s and φss,s with Vs30 and of φss,s with the number of records per site. These results are at PGA, for the relocated dataset, using a GMPE with quadratic scaling and Vs30 as a site proxy.

Our first goal here is to reduce ergodic aleatory uncertainty, i.e. the standard deviation σ, as much as possible through existing information. First we investigate effects related to the source. These should mostly affect the τ component of σ. We examine the effect of our source parameter quality and of the source scaling of the model we use to predict ground motion. In this first step, we will assume that we have no information as to the type of sites are stations are located on (the coefficients of the 'S' term in the functions is 0). We first use a simple prediction model, similar to the formulations of existing models in Greece (e.g. Skarlatoudis et al., 2003 and 2004), as per equation 3.1:

$$f = b_1 M + b_2 \ln(R_{rup} + b_3) + b_4 S + b_5 \quad (3.1)$$

where f is the natural (not decimal) logarithm of the spectral acceleration.
The mixed effects regression yields the bi coefficients and the standard deviations. The latter are shown in the first column of datapoints in Figure 3.3 (left panel). The value of τ is about 0.45 for PGA. We then try to improve our prediction model by introducing a typical, yet still relatively simple, NGA-type model including quadratic scaling and magnitude-dependent geometric spreading. The new formula is:

$$f = b_1 M + b_2 M^2 + (b_3 + b_4 (M - 6)) \ln(R_{rup} + 10) + b_5 R_{rup} + b_6 S + b_7 \quad (3.2)$$

The new standard deviations computed from this model are shown in the second column of datapoints in Figure 3.3 (left panel). τ has decreased, though not significantly, possibly because for our small magnitudes these effects are rather small. Our next step is to improve the quality of the source parameters we used. Our model uses distance and magnitude, and these were initially retrieved from monthly seismic bulletins

(see Chapter 2), which implies automated location of events and magnitude estimation. This is the poorest data quality one may assume to have. Now we use the new source parameters developed in the previous chapter following relocations, catalogue cross-correlations, spectral analyses for magnitude re-estimation, etc. These should improve the source-related error and decrease τ. Indeed, in the third column of datapoints in the figure we see that τ has decreased to 0.29 for PGA. This shows us that at that frequency, an improvement in the dataset can yield an improvement in τ of the order of 30%. While τ has been decreasing during this process, we observe that φs2s and φ do not change, and the improvement in σ is entirely due to the improvement in τ. It should be noted that at longer periods, e.g. at 1 s (lower left panel of the same figure), the overall value of τ (as is typical) is larger, and the improvement in τ is of the order of 50%.

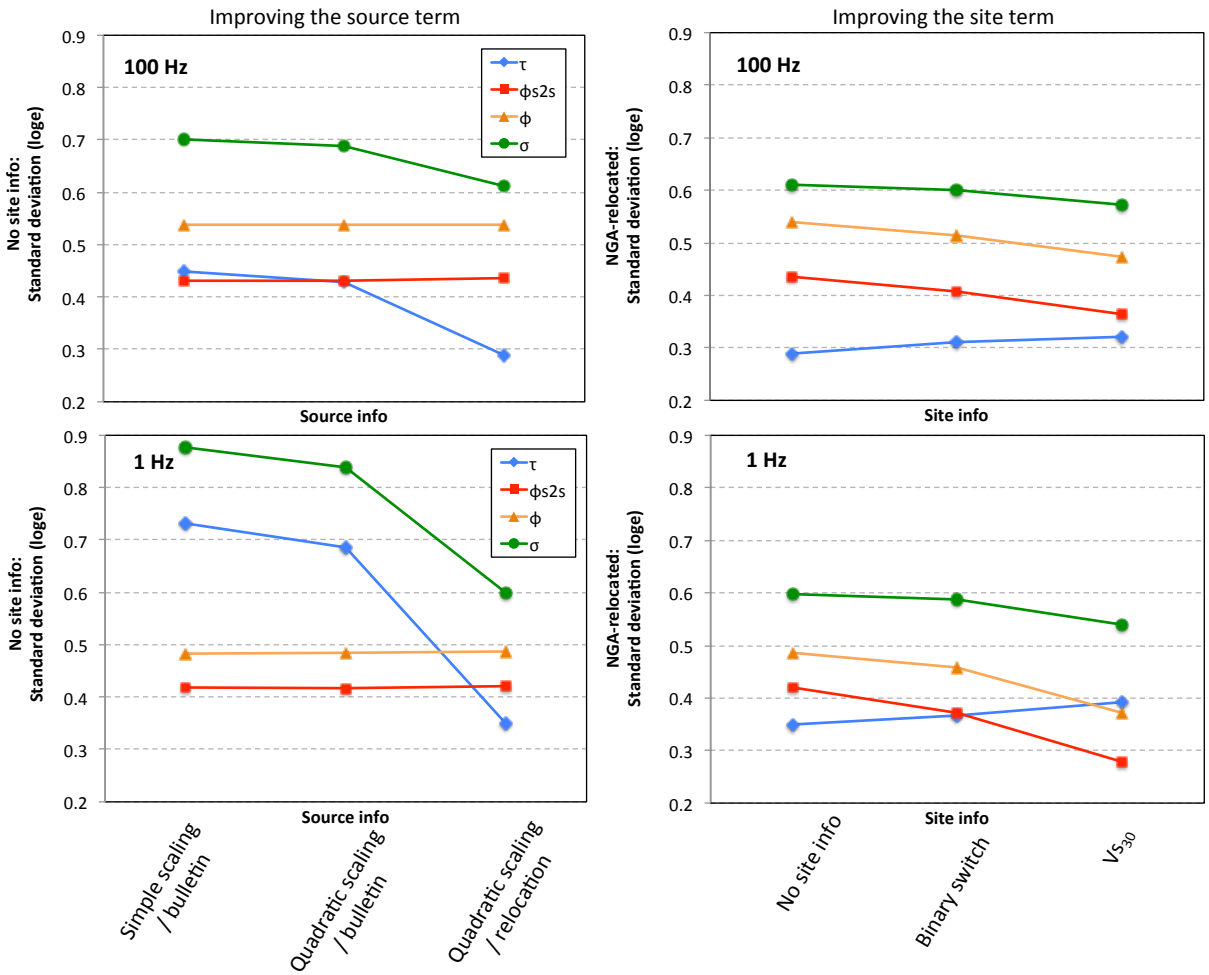

Figure 3.3. Left: The decrease of τ (and hence of σ) with the improvement of source parameter knowledge and magnitude scaling (for the ergodic case, assuming knowledge of Vs30). Right: The decrease of φS2S (and hence of φ and σ) with the improvement of site parameter knowledge (for the ergodic case, assuming revised source parameters and magnitude scaling). Values are shown for 100 Hz (top) and 1 Hz (bottom).

Our second goal is to reduce uncertainty related to the site response, so we seek to simulate a gradual

improvement in site information, and expect it to primarily affect the φ component of aleatory uncertainty. Our previous tests assumed no site information, so our GMPE did not account for differences in sites. Now we introduce a switch to differentiate between soil and rock. This is roughly the actual state of practice in Greece, where switches are implemented based on soil classification (e.g. Skarlatoudis et al., 2003 and 2004). In the right-hand panel of Figure 3.3, this takes us from the first to the second column of datapoints, and it is now the φs2s component, the systematic site-to-site variability, that decreases by 10% for PGA. Next we replace the soil/rock switch by the actual measured value of Vs30, which is the typical way of accounting for site response in current GMPEs. This brings about an additional decrease of φs2s by approximate 10% more for PGA, which in turn leads to a reduction in φ and σ. For longer periods, the overall improvement is larger, about 30%. Here we observe that while φs2s decreases, τ somewhat increases. This is because the two quantities are anticorrelated, and in our dataset -as in most- it is inevitable to have some correlation between parameters (e.g. between magnitude and distance, as is clear by Figure 1.3).

After optimising the global standard deviations, we turn to single-station uncertainty. A global GMPE can be used with these lower global sigmas if the source and site information is as good as possible. However, in order to use non-ergodic sigma values, site-specific estimates must be made for the site terms, using either empirical or numerical methods. With that in mind, we show the values computed for single-station φ and σ, φss and σss, in the fourth column of datapoints in Figure 3.4.

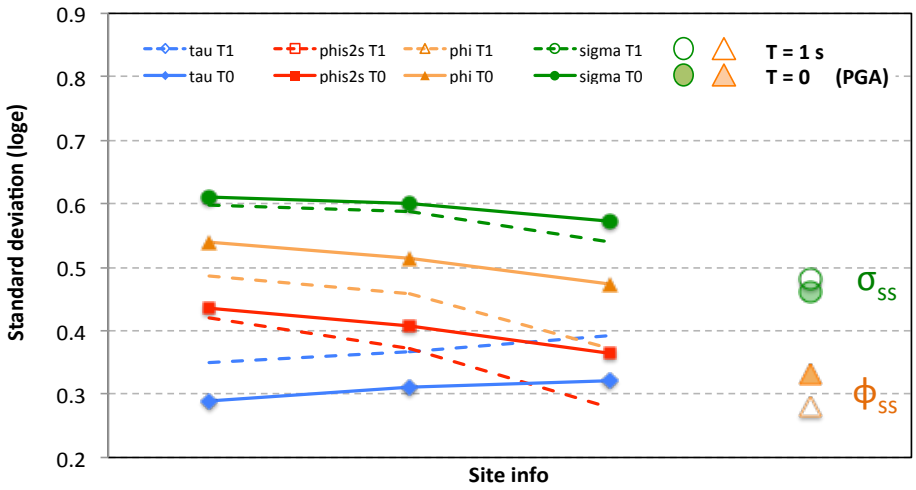

Figure 3.4. The decrease of φS2S (and hence of φ and σ) with the improvement of site parameter knowledge (for the ergodic case, assuming revised source parameters and magnitude scaling) and the passing to non-ergodic values within a site-specific analysis context. Values are shown for 100 Hz and 1 Hz.

In Figure 3.5 we compare the values we have computed at PGA with results retrieved from literature (Boore and Atkinson, 2008; Faccioli & Chen, 2013; Lin et al., 2011; Rodriguez-Marek et al., 2011 & 2013; Luzi et al., 2014; Ornthammarath et al., 2011; Chen & Tsai, 2002; Atkinson, 2006; Chiou & Youngs, 2008; Morikawa, 2008; Anderson & Uchiyama, 2011; Alatik, 2013). Overall, the values we compute for φss, τ, σ,

φss are lower than most published results. For this reason we also plot some typical values for single-path standard deviations, σsp, to show that our results lie between typical single-station and single-path values. We will look into the single-path concept later in the next section.

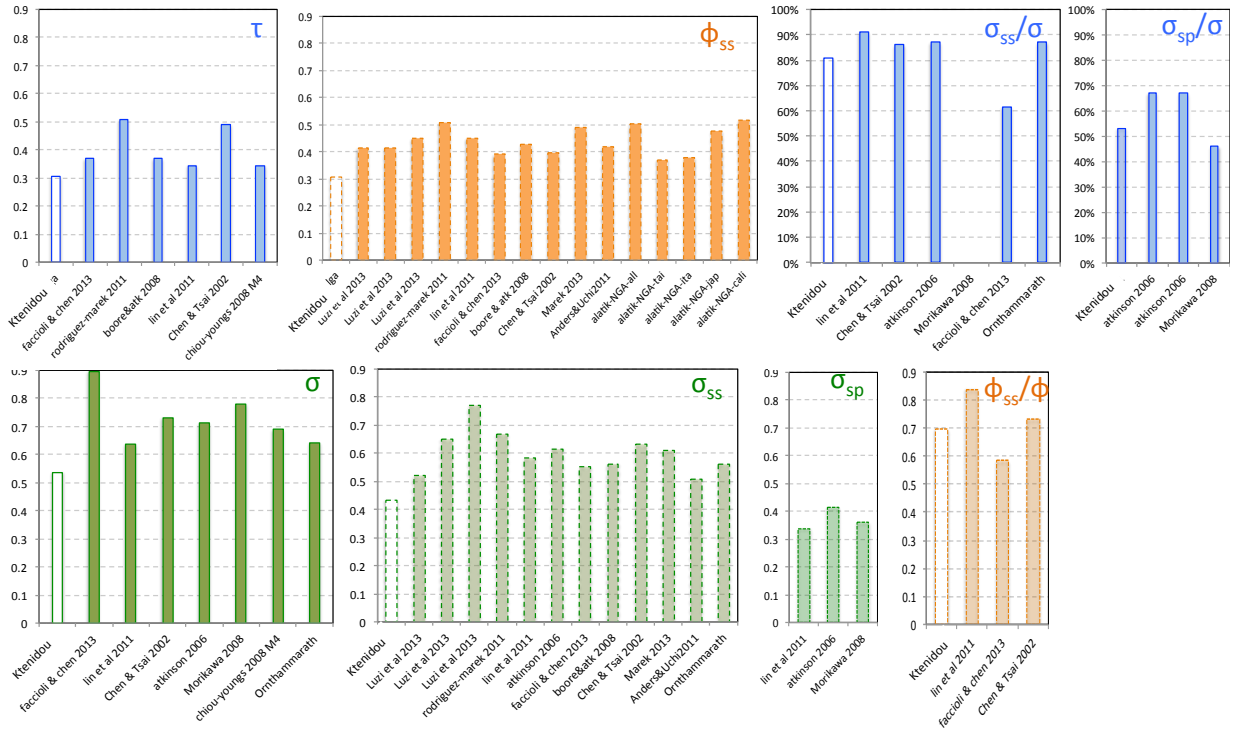

Figure 3.5. Comparison of the results of this section (first bar in each panel) with results from published studies. All values pertain to PGA (T=0) and are natural logarithms.

2.2 Single station standard deviations: stability, dependencies and site variability

In the previous section we presented results for two selected periods, PGA and 1 s. Figure 3.6 shows the dependence of global and single-station uncertainty components with period, from 0.01 s up to 2 s. Looking at longer periods, our dataset decreases. This is because we only use data within its range of validity and we do not compute spectral accelerations outside the filtering frequencies mentioned in Chapter 1 (Figure 1.7), i.e. we have no data below the lowest usable frequency. Compared to the data we can use at high frequencies, at 1 s we have already lost roughly half our data in terms of records and events, and at 2 s we have lost over 2/3 of them. This is why we do not show any results for periods longer than 2 s.

The gradual increase in τ is often observed as periods grow longer. It is reasonable given the decrease in the number of earthquakes we can use at long periods. As is often observed, τ and φ are anti-correlated, and we see this here, where φ decreases as τ increases. We observe a spike in φ and φs2s values around 1.3-1.6 Hz. These frequencies correspond to the resonant frequency of some of the sites in this study, and

the spikes indicate an increase in variability due to site response due to the different resonances. At PGA, the ratio of σss/σ is near 80% and the ratio of φss/φ is near 70%. These are somewhat lower than some published values, and this may indicate that our dataset has somewhat stronger site terms than usual sites.

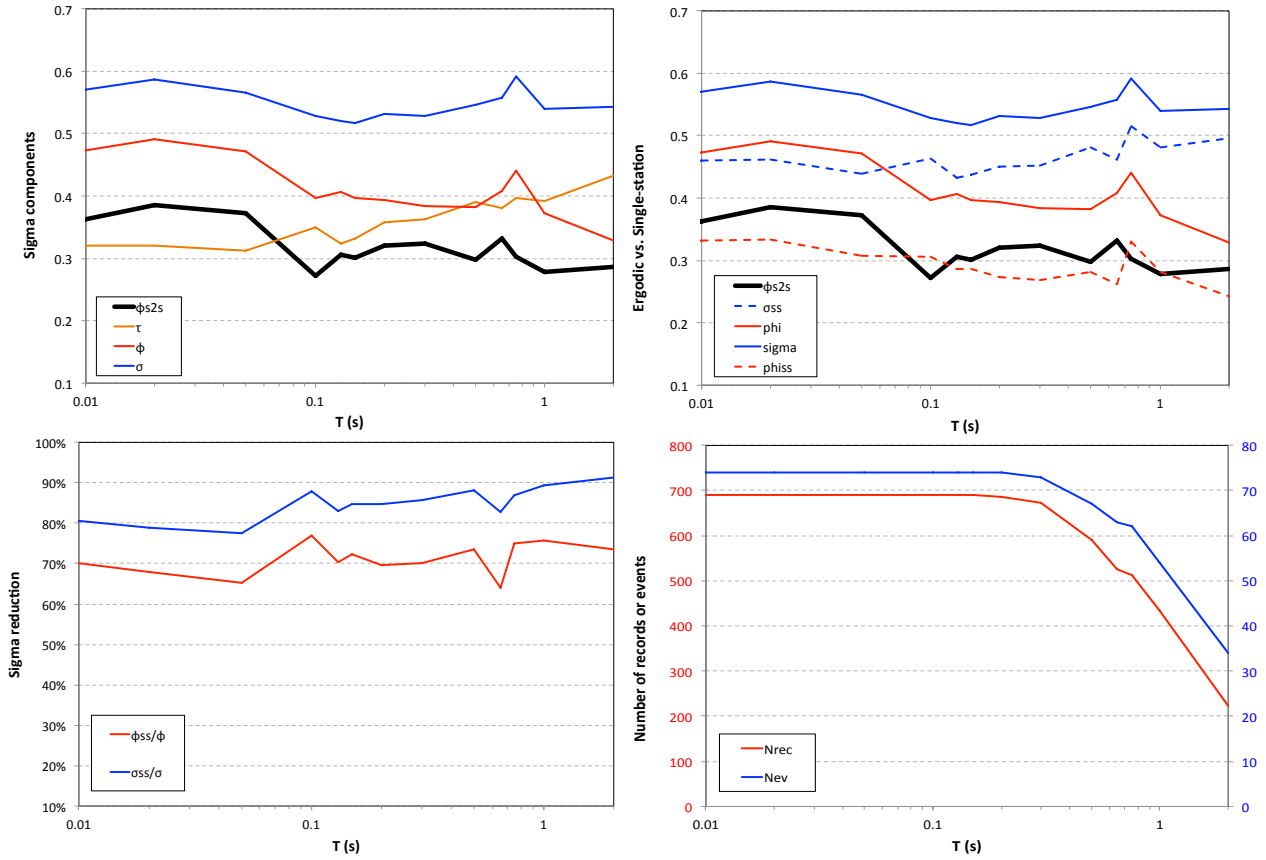

Figure 3.6. Dependence of uncertainty components with period (upper panels and lower left). Decrease of the number of records and events with period (lower right panel).

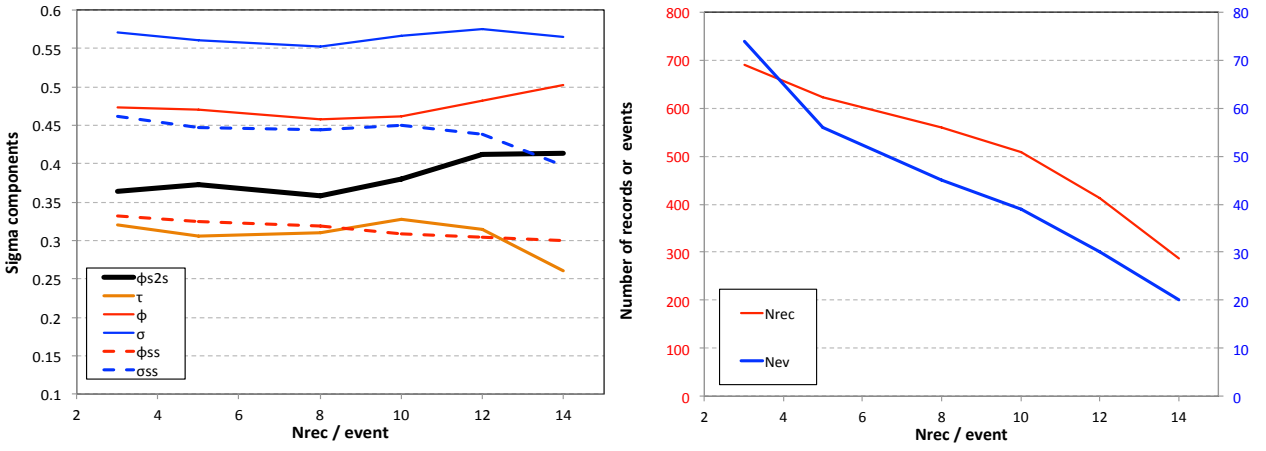

Figure 3.7. Dependence of uncertainty components with the criterion of minimum required number of records per event. Results are for PGA.

The number of records used may have an effect on our results. In this study we used a criterion for the minimum number of records per event, which we set at 3, the minimum value typically allowed in such studies. We check the robustness of our estimates by running a parametric analysis for PGA, where we shift this criterion towards stricter values, namely 5, 8, 10, 12, and 14 (Figure 3.7). The results are very stable from 3 up to 8 records per event. If the criterion becomes stricter than 10, then τ decreases, as expected, since each event term can be even better determined. The downside of this is that there are fewer events left in the dataset (half or less), as shown in the figure on the right. If the criterions becomes stricter than 10, the φs2s increases slightly. This has been observed before, and for the US this increase is of the order of 10% (N. Abrahamson, personal communication), which is similar to what we see here. Finally, we keep our criterion value at 3. This value gives us a good estimate of all components of uncertainty, without sacrificing any of the data, especially as this would have a heavy effect on longer periods.

Another aspect of interest to the stability and robustness of our estimates is the question of representation of different site types in the dataset. As we mentioned in Chapter 1, rock and soil sites are not represented equally, as is almost always the case. Added to the magnitude-distance correlations in our dataset, this may cause further trade-offs between τ and φ. We compute the average Vs30 per event, as an index of the prevalent type of station that recorded each event. In Figure 3.8 we plot our dBe residuals for each event against this average Vs30 value: e.g., for 300 m/s, the event was recorded mostly by soft soil stations, while for 800 m/s, the event was recorded by mostly rock stations. The latter case is very rare, but it is evident from the plot that there is some correlation between residuals and Vs30 values. This correlation is still there even if we use a stronger minimum record per event criterion, e.g. 10 rather than 3. This indicates that there are likely some correlations in our dataset between source and site terms, but –as in most datasets– this cannot be overcome.

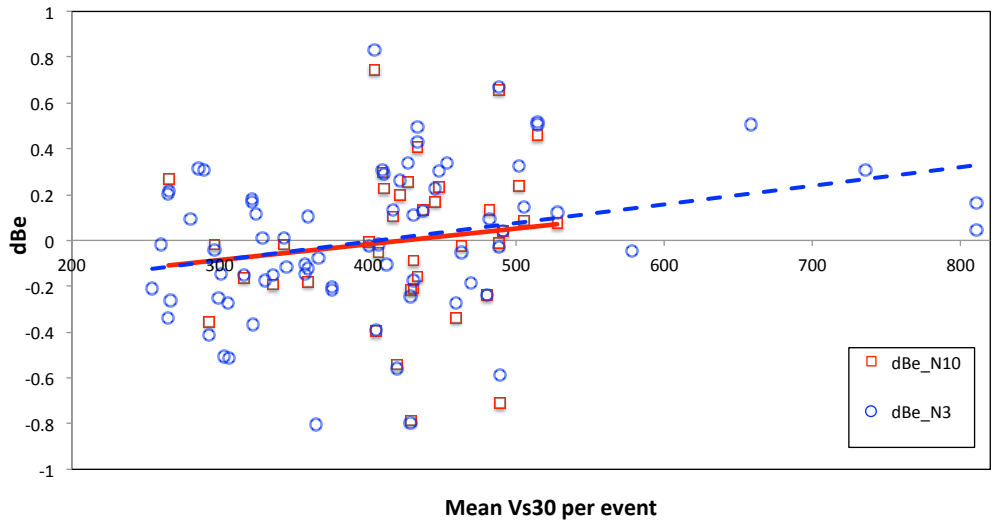

Figure 3.8. Dependence of between-event residuals with the averaged Vs30 per event for different minimum records per event criteria.

After discussing the robustness and stability of the results, we proceed to observe tendencies in our results, and understand dependencies with various parameters. First we use the φss,s results to find which sites have the strongest and weakest variability in EUROSEISTEST. In Figure 3.9, we plot the stations of our array, colour-coded as to their φss,s values, at different frequencies: PGA, 1 Hz and 2 Hz. In the plots, the scale from blue to orange orders stations from the least to the most variable. The plots indicate that the stations in the EW axis are less variable overall than some of the stations along the NS axis. Station PRO_000 has the highest φss,s at high frequencies, but is rather stable at low frequencies. This could be related to topographic effects, as it is the only station of the array located on a hill. Station TST_196 has the highest φss,s at 1 Hz. The resonant frequency of the soil column at TST is close to 1 Hz, so this could be related to the presence of a downgoing wavefield. The variability near the basin edges along the NS axis (stations PRR, STC) could be related to basin edge and lateral discontinuity effects (see structure in the lower panel of the figure), but if it is so, it is not clear how it behaves with frequency. The variability of most other stations is harder to speculate upon without complementing these results with simulations.

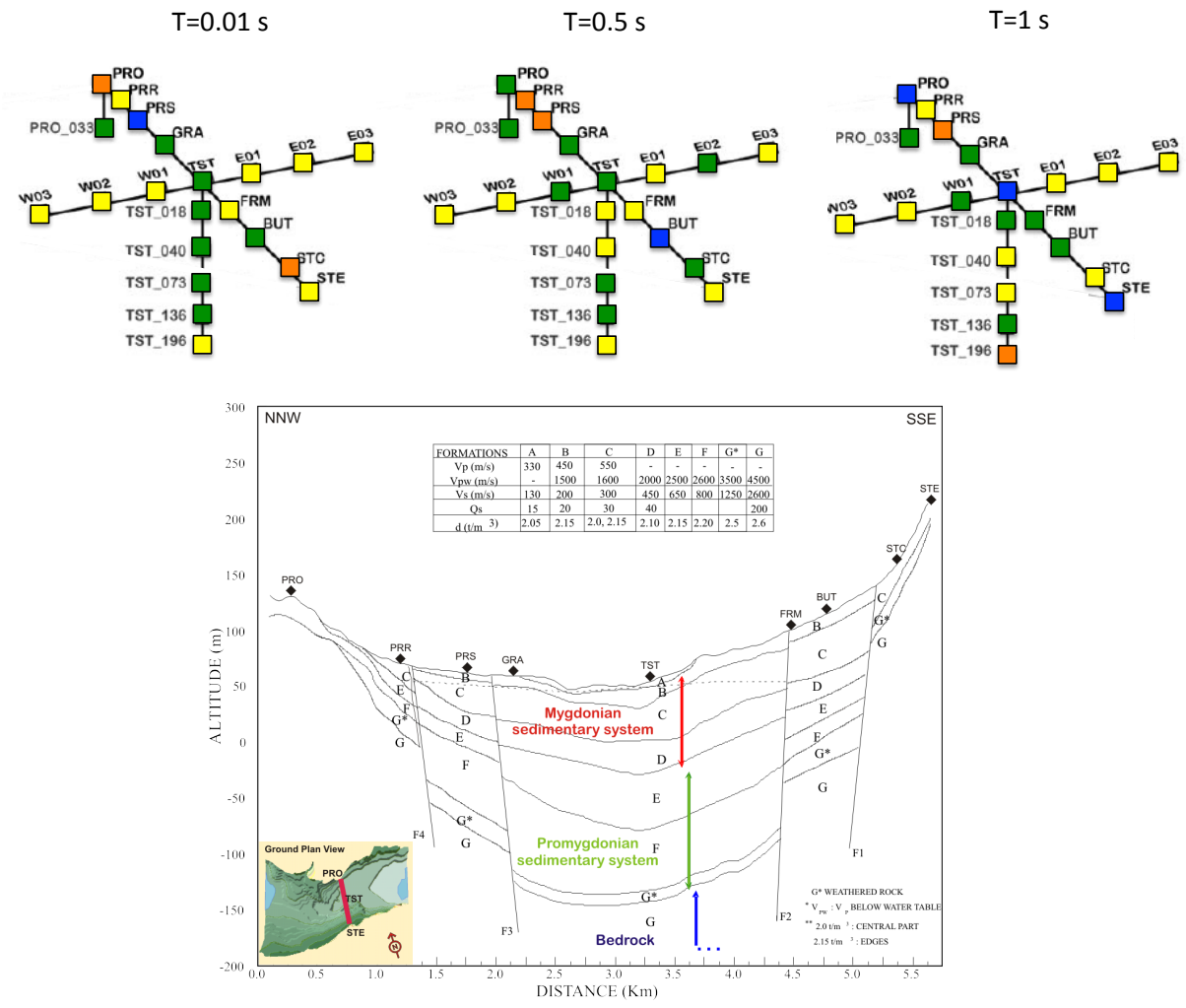

Figure 3.9. Top: The array stations colour-coded with respect to their variability (φss,s) for PGA, 1 Hz and 2 Hz. Blue is for least and red is for most variable stations. Bottom: Sketch of the geology beneath the array (http://euroseisdb.civil.auth.gr/2dstruct).

At this point is it useful to look at how the site-related variable in the GMPE can affect results. Figure 3.10 shows the δs2s, i.e. the systematic deviations from the average site response scaling for each site, for the three GMPE cases presented in the first section: a model with no site information, one with a soil-class switch to differentiate site response, and one with Vs30 as a proxy for site response scaling. We focus on the stations in the two boreholes, PRO and TST. The only stations for which δs2s values change noticeably between models are PRO_000 and the hard rock downhole stations, PRO_33 and TST_196. In the first case (no site variable), the δs2s values are rather representative of actual site response, so the two downhole rock stations plot below any of the stations overlying them. However, when models include a site variable, the φs2s values do not indicate relative site response, but rather the deviation from the response predicted for the particular site class or Vs30. In other words, the δs2s values indicate how far the prediction is from reality, and if the deviation is large, then this means that there would be a lot to be gained from site-specific analyses in lieu of site class- or Vs30-based predictions. Here, we notice that the data point for TST_196 moves towards 0 as the models site variable becomes more refined. This indicates that use of Vs30 in the model improves the prediction. On the other hand, the two stations at PRO tend to move farther away from 0 as the models become more refined. This is an indication that the actual response is far from the average response predicted for their site classes. The possible effect of the GMPE on φs2s will be discussed again in the last section of this chapter, when we test different existing models to compute single-station sigmas.

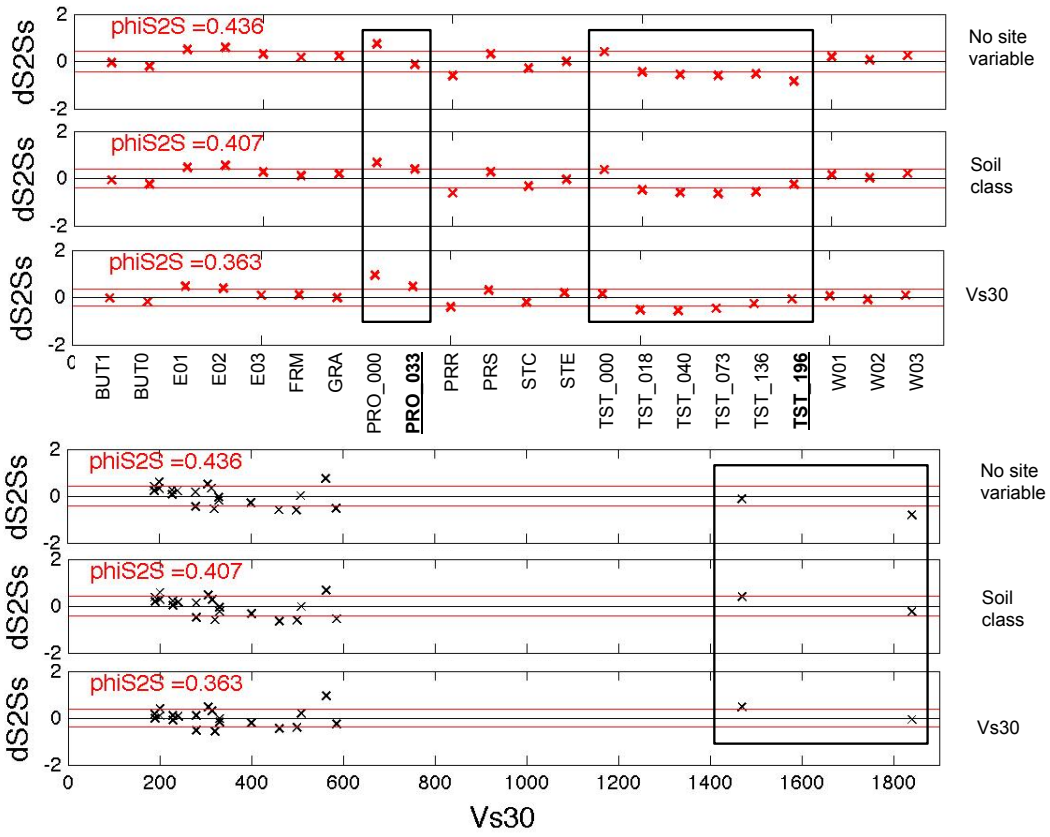

Figure 3.10. The effect of the site-related variable in the GMPE (no site information, site class switch, or Vs30) on δs2s,s, at PGA (top) and the correlation of the residuals with Vs30 (bottom).

We now turn to dependencies of the between-event and the corrected within-event residuals with parameters such as magnitude, distance, and depth (Figure 3.11). Global datasets have shown certain trends with magnitude and distance, but their magnitude range is well above the magnitudes of our dataset, so it is interesting to see to which extent we can detect such trends in our data. The figure shows that τ tends to decrease for smaller magnitudes, and that this tendency is stronger for longer periods. This tendency has been observed before but is generally not considered. It could be related to correlations between source and site terms, possibly due to the fact that for very small magnitudes, kappa may often mask the true corner frequency of the source. Conversely, φss tends to increase for smaller magnitudes, and this is clearer for higher frequencies. This effect has been observed before down to M4.5 (e.g. Rodriguez-Marek et al., 2013), and is seen here to hold also for magnitude ranges down to M2. There are several possible reasons for this effect, including poor locations and depth estimates for very small events, or higher stress drop variability and kappa effects, which may cause some of the source uncertainty to map onto φ. The correlation of φss with distance is not as clear. For shorter distances, φss seems to decrease at longer periods and increase for higher frequencies. The latter is found by Rodriguez-Marek et al., 2013. To the extent that events recorded at short distances are generally small events, this latter tendency is consistent with the previous observation. Finally, the dependency with depth is not very clear either, but φss seems to increase slightly for shallower events at longer periods. This could be related to oblique incidence of the incoming waves onto the basin edges in the case of very shallow events. However, depth is the least constrained parameter and we can merely speculate as to its effect.

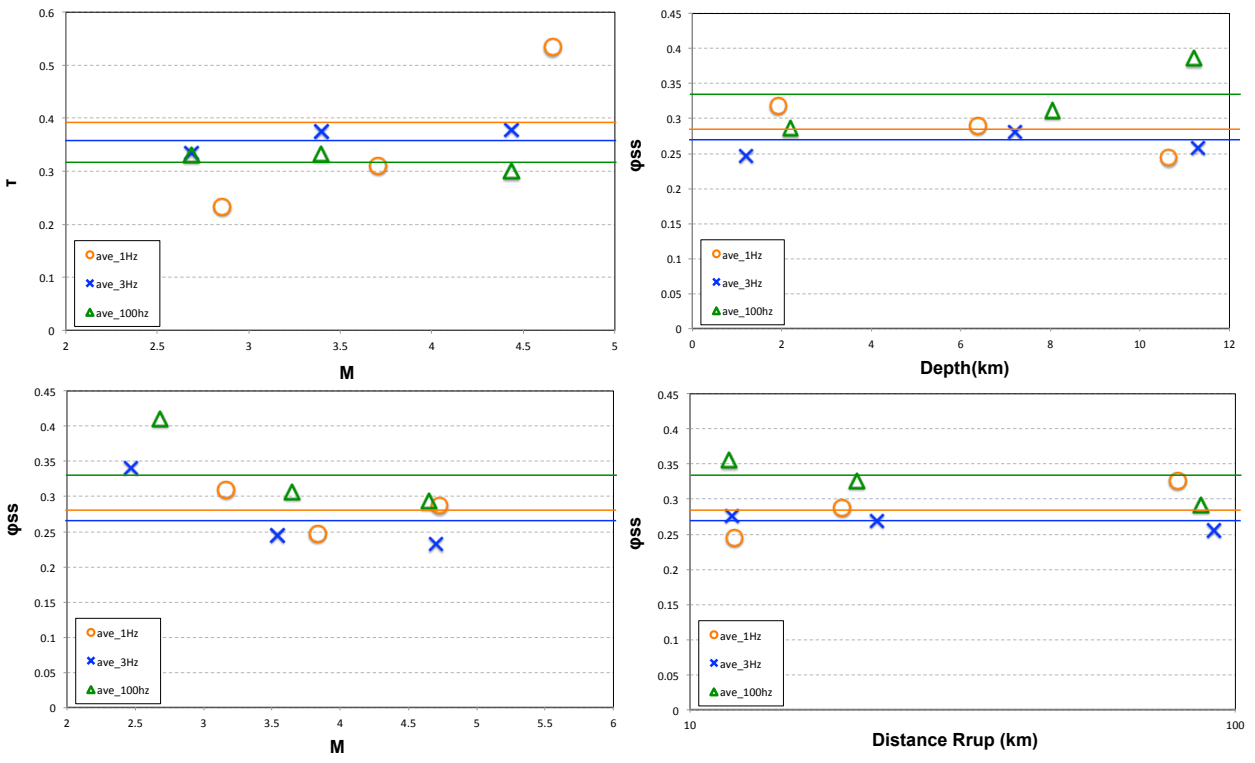

Figure 3.11. Dependencies of τ and φss on magnitude, distance, and depth at PSA, 1 Hz, and 2 Hz. The solid lines indicate the average value and the symbols are the binned values.

Another possible interpretation for the increase of site variability for small events compared to large ones has to do with the azimuthal coverage. As seen in Figure 1.4, larger events seem to lie on certain paths with respect to the site, while small events tend to surround the site better. Poor azimuthal coverage may lead to poor path sampling and hence to lower variability for larger events, while the good coverage may lead to better sampling of all paths surrounding the site, and hence higher variability for smaller events.

This is difficult to quantify. One index that has been proposed is the closeness index (CI) defined by Lin et al. (2011). Following the methodology those authors lay out, we compute the closeness index for each pair of events recorded by each station, together with the normalized difference in the within-events variability for each pair of events (Figure 3.12). We compute the average CI per station and find that they range from 1.3-1.6. According to the methodology, a CI higher than 1 indicates that there are no significant single-path effects that would decrease the φss towards φsp. However, Figure 3.13 shows that larger events (red points, M>4.5) are clearly located on certain azimuths from the site, while smaller events (green points, M<3) sample more azimuths around the site.

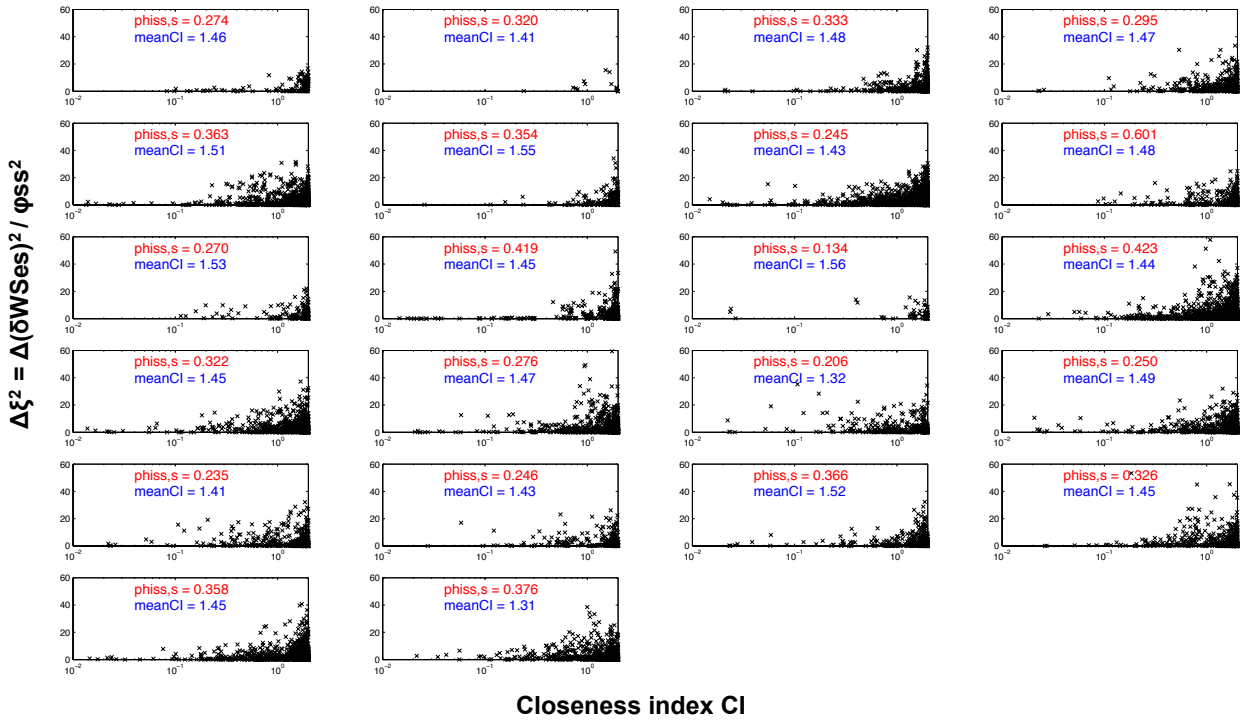

Figure 3.12. Closeness index and squared normalised differences in within-events residuals, computed for each pair of events recorded at each station of the array. The average CI per station is marked in blue.

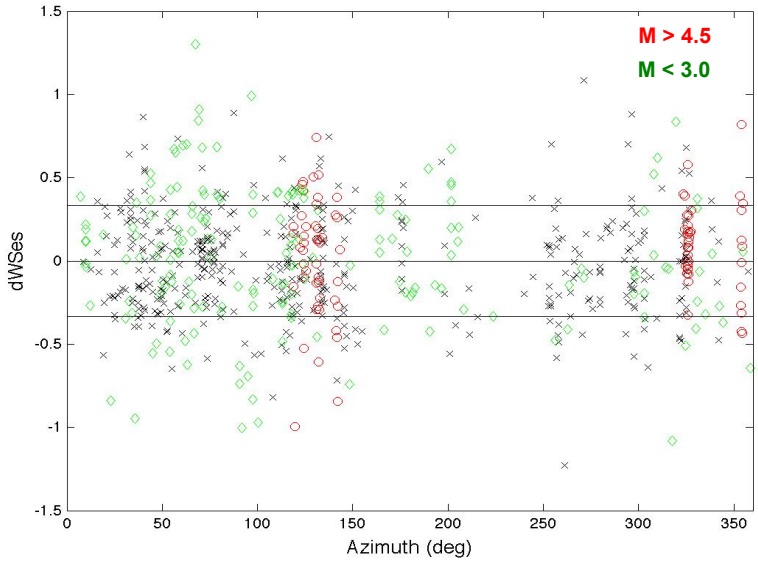

Figure 3.13. Distribution of within-event residuals with azimuth, colour-coded as to magnitude.

2.3 Using existing GMPEs

We have made this study of residuals and standard deviations by first fitting a simple GMPE to our dataset to compute the mean, then taking out this mean, and working with the residuals in order to study the components of aleatory uncertainty. This decision is based on the notion that ground motion variability seems to be a fundamentally robust feature globally, but may have regional dependencies with magnitude and distance. Furthermore, what is most important in our case, our dataset lies for the most part outside the range of validity of most existing GMPEs, at least those made for seismically active regions. Importing an existing GMPE made for magnitudes mostly above 4.0 or 4.5 will inevitably cause trends in residuals with respect to magnitude, and possibly with distance. This in turn will most probably inflate the between-event uncertainty (τ), but as τ is correlated with within-event uncertainty (φ), it is not certain that φ or φss will remain unaffected. Furthermore, any errors in distance scaling will in all probability map onto φ. Hence, fitting a GMPE that is exactly centred on our data is the most secure approach to computing well-balanced within-event and between-event residuals to work with.

In this section we investigate another approach, namely the possibility of using existing global GMPEs for the purpose of computing single-station variability (this was done e.g. by Chen and Faccioli, 2013, for New zealand). Of the very large number of existing models, we choose a few representative ones based on certain criteria:

- Akkar et al. (2014), as an example of the most recent generation of European models from the RESORCE database,
- Bindi et al. (2011), as a European GMPE which contains a considerable amount of data between M4.0-M4.5,

- Danciu and Tselentis (2007) and Skarlatoudis et al. (2003), as the most recent models developed for crustal events in Greece, and
- Skarlatoudis et al. (2004), as a model specifically developed for smaller magnitudes in Greece.

Table 3.1 presents some of the salient characteristics of these models, including magnitude and distance range, distance metric, style-of-faulting (normal, reverse, strike-slip, and thrust), use of quadratic scaling, site characterisation information. Many of these models predict quantities outside the scope of the present study, so in the last column we only mention whether they predict SA at a full range of periods or merely PGA. We note that Skarlatoudis et al. (2003) proposes two formulae for PGA from large events (which we denote as a and b), while Skarlatoudis et al. (2004) proposes two formulae for PGA from small events (which we denote as a and b) and one for the mixed dataset of small and large together (which we denote as x).

We analyse the residuals between the predictions of these models and our relocated dataset. We assume normal faulting mechanisms for our events, as this is by far the prevalent mechanism in the region. We use R_{hyp} for Akkar et al. (2014) and R_{epi} for all other models. We are interested first in observing how each model's scaling fits our dataset, and secondly in whether any scaling problems are 'absorbed' by the between-event uncertainty (τ) and possibly by the systematic deviation from average site scaling (φs2s), so as to allow an adequate estimate of the single-station variability, φss.

Table 3.1. Comparison of the salient features of the following GMPEs: Akkar et al. (2014), Bindi et al. (2011), Danciu and Tselentis (2007), Skarlatoudis et al. (2003), and Skarlatoudis et al. (2004).

#	Model	M_w	R	R type	Site variable	SoF	M^2	T range
1	ASB14	4.0-7.5	200 km	R_{jb}, R_{epi}, R_{hyp}	Vs_{30}	N, R, SS	Yes	SA(T)
2	Bindi11	4.0-6.9	200 km	R_{jb} (R_{epi} if M<5.5)	Site class	N, R, SS, Unknown	Yes	SA(T)
3	Danciu	4.5-6.9	136 km	R_{epi}	Site class	N, SS/Thrust	No	SA(T)
4	Ska03ab	4.5-7.0	160 km	R_{epi}	Site class	N, SS/Thrust	No	PGA
5	Ska04ab	1.7-5.1	40 km	R_{epi}	None	None (mostly N)	No	PGA
	(Ska04x)	*(1.7-7.0)*	*(160 km)*					*(PGA)*

Figure 3.14 shows a comparison of all the standard deviation components (τ, φ, σ, φs2s, φss, σss) computed at all periods available using the chosen GMPEs. The standard deviations computed in the first part of this study, where we fit a new GMPE to the data, are shown for comparison. The first observation is that the φss seem practically independent of the model used, as all datapoints coincide for each period. The systematic deviation, φs2s, is rather stable for PGA, but at longer periods exhibits some discrepancies between existing models and our model, as well as between individual existing models. These discrepancies are stronger as periods become longer and will be discussed later. But the most striking discrepancy is between τ values, which appear to be strongly dependent on the model used. All models show larger τ values than what we achieved by fitting a new GMPE, especially around 2-10 Hz. Up to 1 s, the model of Akkar et al. (2014) shows the largest increase in τ, while that of Danciu and Tselentis (2007)

lies closest to the τ of the new GMPE.

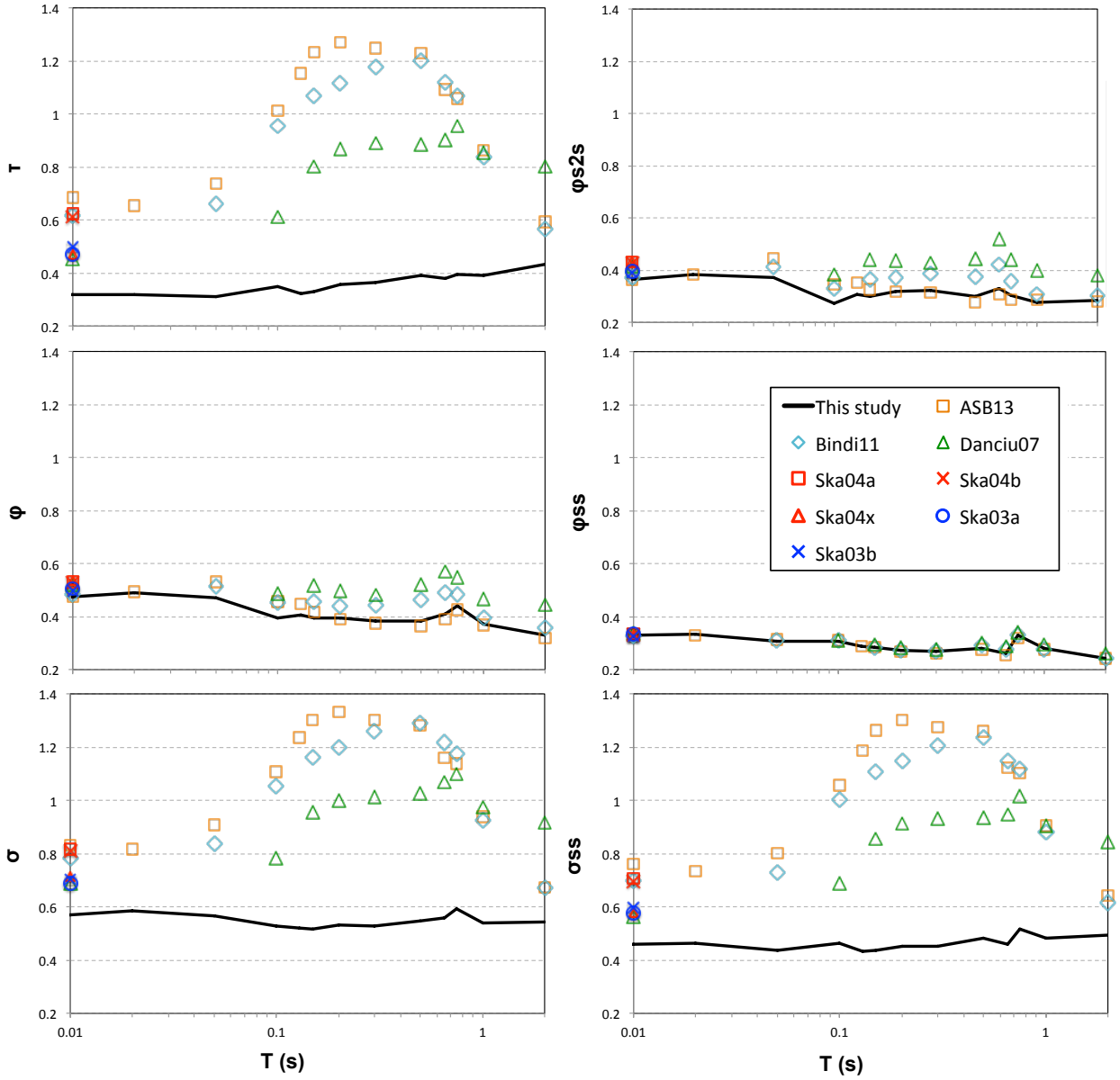

Figure 3.14. Comparison of the standard deviation components (τ, φ, σ, φs2s, φss, σs) as computed at all periods available using the following GMPEs: Akkar et al. (2014), Bindi et al. (2011), Danciu and Tselentis (2007), Skarlatoudis et al. (2003), and Skarlatoudis et al. (2004). The standard deviations computed in the first part of this study, fitting a new GMPE to the data, are shown by the black solid line. We note that the φss is practically independent of the model used, while τ is very strongly dependent on the model. All models show much greater τ values than what we achieved by fitting a new GMPE. Up to 1 s, the model of Akkar et al. (2014) shows the largest increase in τ, while that of Danciu and Tselentis (2007) lies closest to the results of the new GMPE.

We now study results for individual models in more detail (Figures 3.15 through 3.19). We choose the two models that differ mostly in their τ: we take the closest and the farthest from our initial τ estimate, namely Danciu and Tselentis (2007) and Akkar et al. (2014), respectively. Figure 3.15 compares observed spectral accelerations at PGA (left) and 1 Hz (right) with the predictions of two GMPEs. The models work better at high frequencies, though they consistently overpredict spectral accelerations. Akkar et al. (2014) seems to capture the ground motion only for the events at farther than 80-100 km, which are almost the only events in our dataset within the model's rage of applicability (M4.0-5.0). All other distances are dominated by smaller magnitudes. At longer periods, the overprediction is more severe for all distance ranges. In Figure 3.16 we see clearly that total residuals show trends with magnitude and distance, but not with Vs30. The correlation with magnitude is the strongest. In Figure 3.17 we see this clear trend again in the correlation of between-events residuals (dBe) with magnitude at low and high frequencies. At high frequencies, the correlation is stronger for the Akkar et al. (2014) model. These trends mean that the models do not work well for the magnitude scaling of this dataset. This was to be expected, given that the magnitude scaling becomes steeper as magnitude decreases and our data are beneath typical model magnitude ranges. The next question is whether the errors in magnitude (and possibly distance) scaling may map onto within-event residuals (δWes), given the trade-offs in τ and φ. However, in Figure 3.18 we see no systematic trend of the within-event residuals (δWSes) with distance, which means that there is no detectable inconsistency in distance scaling. Furthermore, φss,s values are not correlated to Vs30 or the number of records. These are indications that the single-station component of uncertainty can be predicted, at least to some degree, using these models, however poorly balanced they are as to their total residuals. However, some discrepancies are observed in individual φss,s values between models, e.g. at station 19 (TST_196). This is because there are differences in how these models treat site amplification, and these differences map onto the systematic deviations (δs2s). In Figure 3.19, the fluctuation of δs2s between stations 14-19 (TST_000 through TST_196, respectively) is stronger for the model of Danciu & Tselentis (2007), most probably due to the fact that this model treats sites using EC8 site classification as a proxy, while the other uses Vs30, a more exact descriptor.

In Figure 3.20 we show δBe residuals for all GMPEs tested, to generalize the observations we made previously for the Akkar et al. (2014) and Danciu & Tselentis (2007) models. Indeed, the magnitude trends are clear for all cases, meaning that there are magnitude scaling issues with all models (surprisingly, even for the Skarlatoudis et al., 2004, models made for smaller magnitudes). However, in Figure 3.21 we see that the δWSes residuals are well balanced with distance. This means that, for all models tested: 1. The magnitude scaling errors were successfully corrected by the event terms; and 2. There is no discernible error in the distance scaling, due to the chosen GMPEs coming form the same or similar region (Greece or Europe). These two conditions are what allows us to compute single-station sigmas despite the obviously large total σ values and the biased total residuals. It should not be concluded from these results that any GMPE from any region could serve just as well to compute single-station variability.

Finally, we look at the differences between models in the final products: φs2s and φss. In Figure 3.22a we focus on PGA, and break up the average values of φs2s and φss into their site-specific values, δs2s and φss,s. We plot these per site and also show the average values for comparison. φss,s is remarkably stable, and models converge the best at the most and least variable sites of the array (PRO_000 and PRS, respectively). φs2s,s is rather stable for most stations, but shows striking variability for stations PRO_033

and TST_196. These happen to be the only two very hard rock sites in the array, located in healthy granite. We note that models that do not account for site information in their formulation (Skarlatoudis et al., 2004) plot far from models that use Vs30 as a predictor variable (our ad hoc GMPE and the Akkar et al., 2014), while models that use a site classification switch tend to plot in between (Skarlatoudis et al., 2003; Bindi et al., 2011; Danciu & Tselentis, 2007). The difference at PRO_033 between our model and Akkar et al. (2014) is significant, but this observation is in line with what we observed before when testing different formulations of our own GMPE (Figure 3.10). Similar observations can be made for the results 1 Hz (Figure 3.22b), i.e. φss,s is again rather stable, while differences in δs2s are even greater at the two hard rock stations.

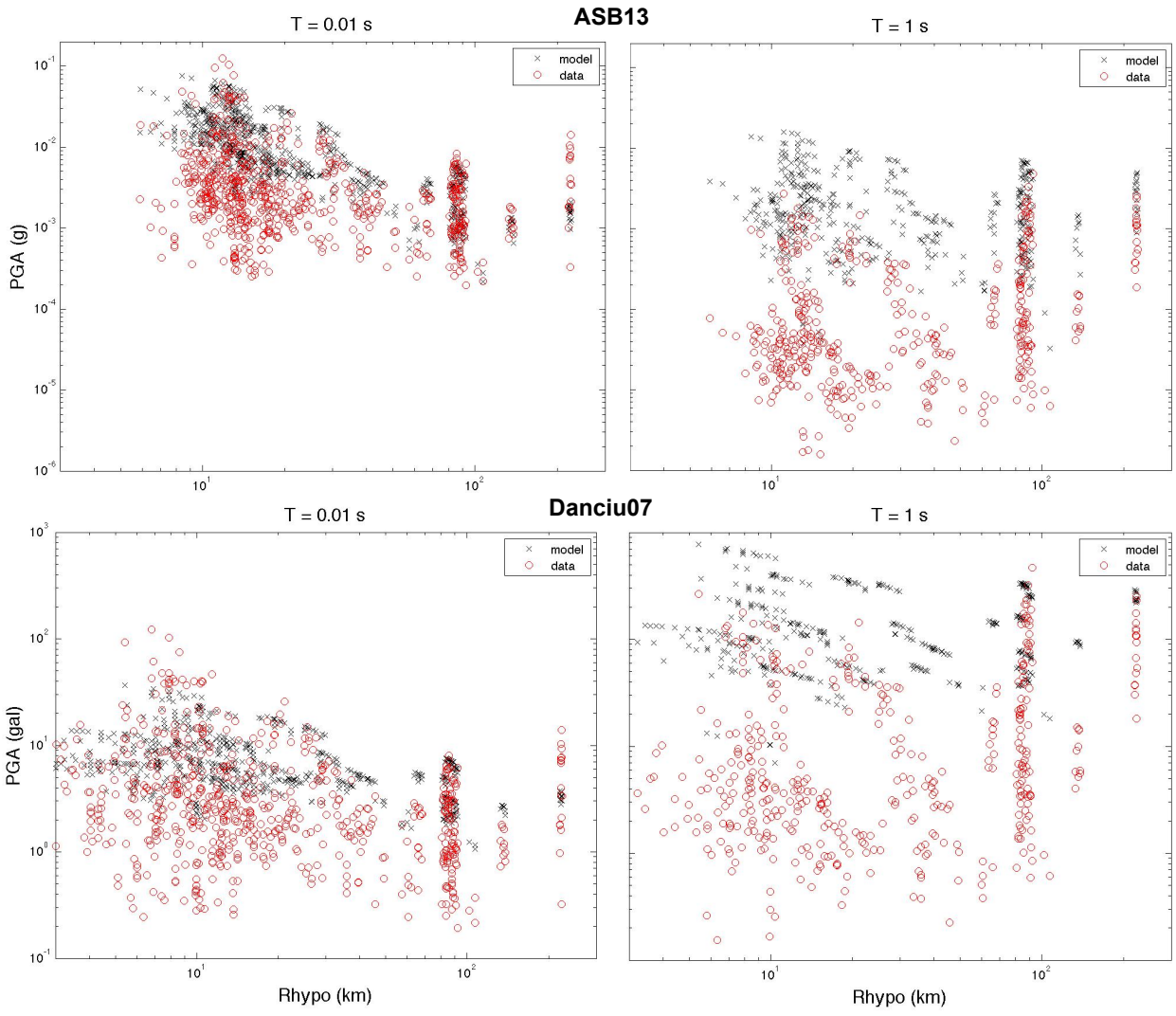

Figure 3.15. Comparison of observed spectral accelerations at 100 Hz (left) and 1 Hz (right) with the predictions of two GMPEs: Akkar et al. (2014), top, and Danciu and Tselentis (2007), bottom. The models work better at higher frequencies, though they consistently overpredict spectral accelerations.

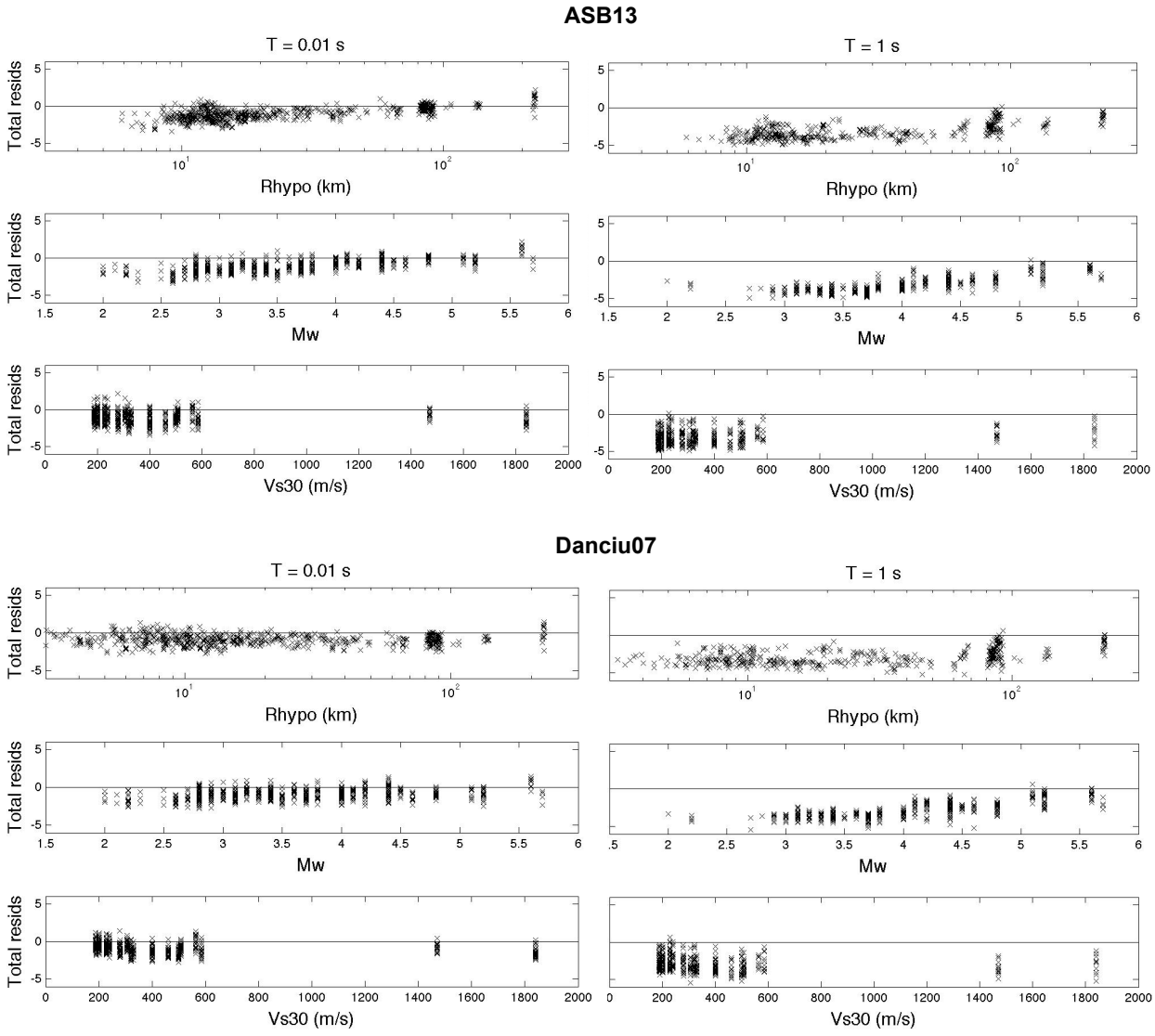

Figure 3.16. Comparison of total residuals between observed spectral accelerations at 100 Hz (left) and 1 Hz (right) and the predictions of two GMPEs: Akkar et al. (2014), top, and Danciu and Tselentis (2007), bottom. The plots show trends of residuals with magnitude, distance and Vs30.

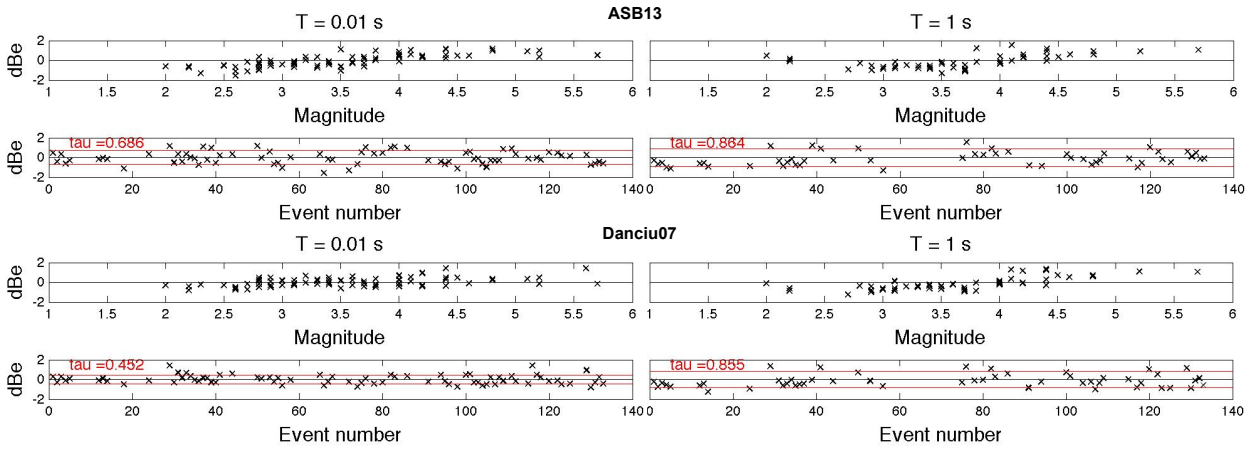

Figure 3.17. Between-event residuals between observed spectral accelerations at 100 Hz (left) and 1 Hz (right) and the predictions of two GMPEs: Akkar et al. (2014), top, and Danciu and Tselentis (2007), bottom. The plots show trends of the residuals with magnitude, indicating that the magnitude scaling of the GMPEs is not adequate for our dataset. The trends are stronger for the model of Akkar et al. (2014).

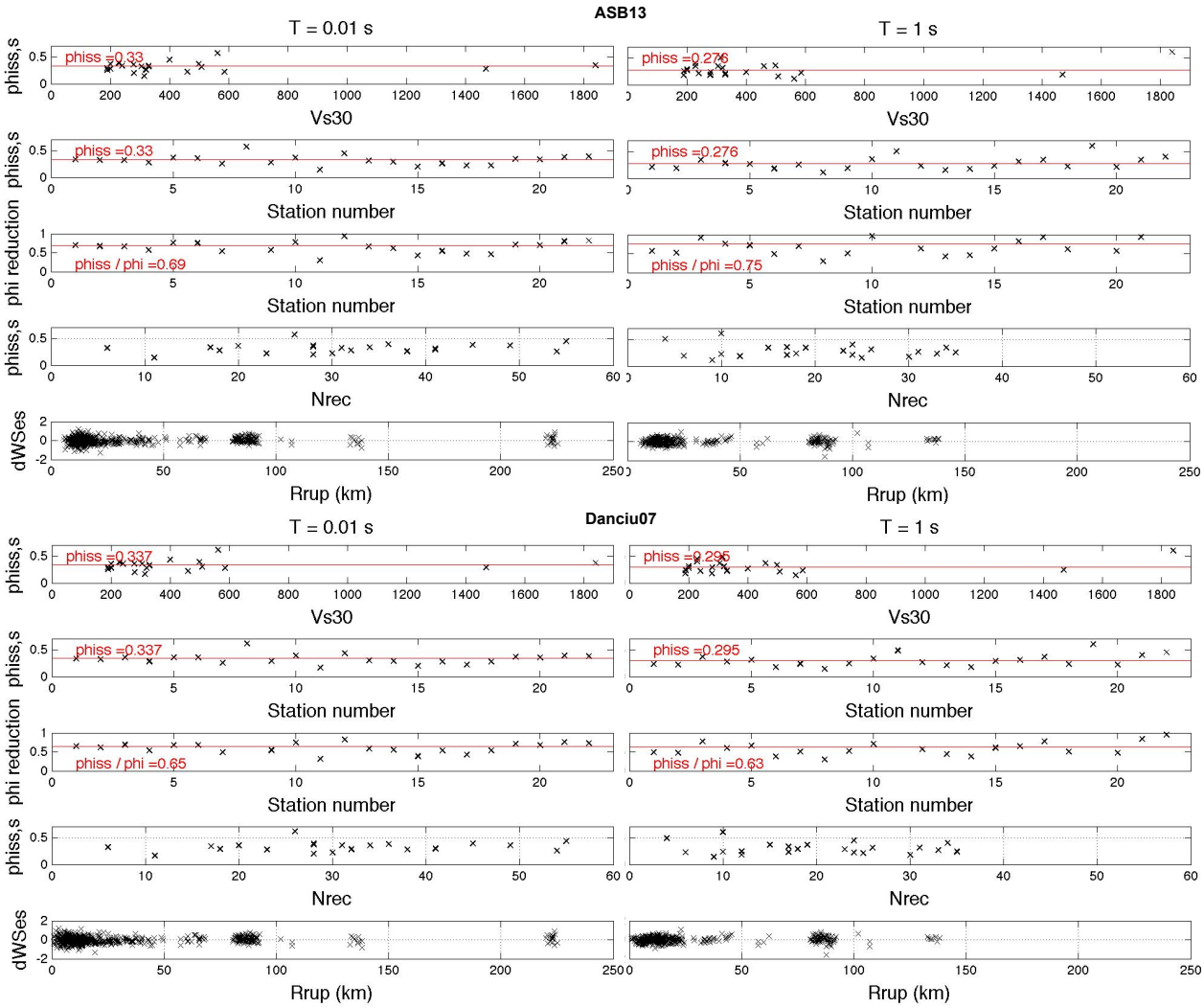

Figure 3.18. Single-station standard deviations between observed spectral accelerations at 100 Hz (left) and 1 Hz (right) and the predictions of two GMPEs: Akkar et al. (2014), top, and Danciu and Tselentis (2007), bottom. The plots show that there is no systematic trend with distance, Vs30, or number of events.

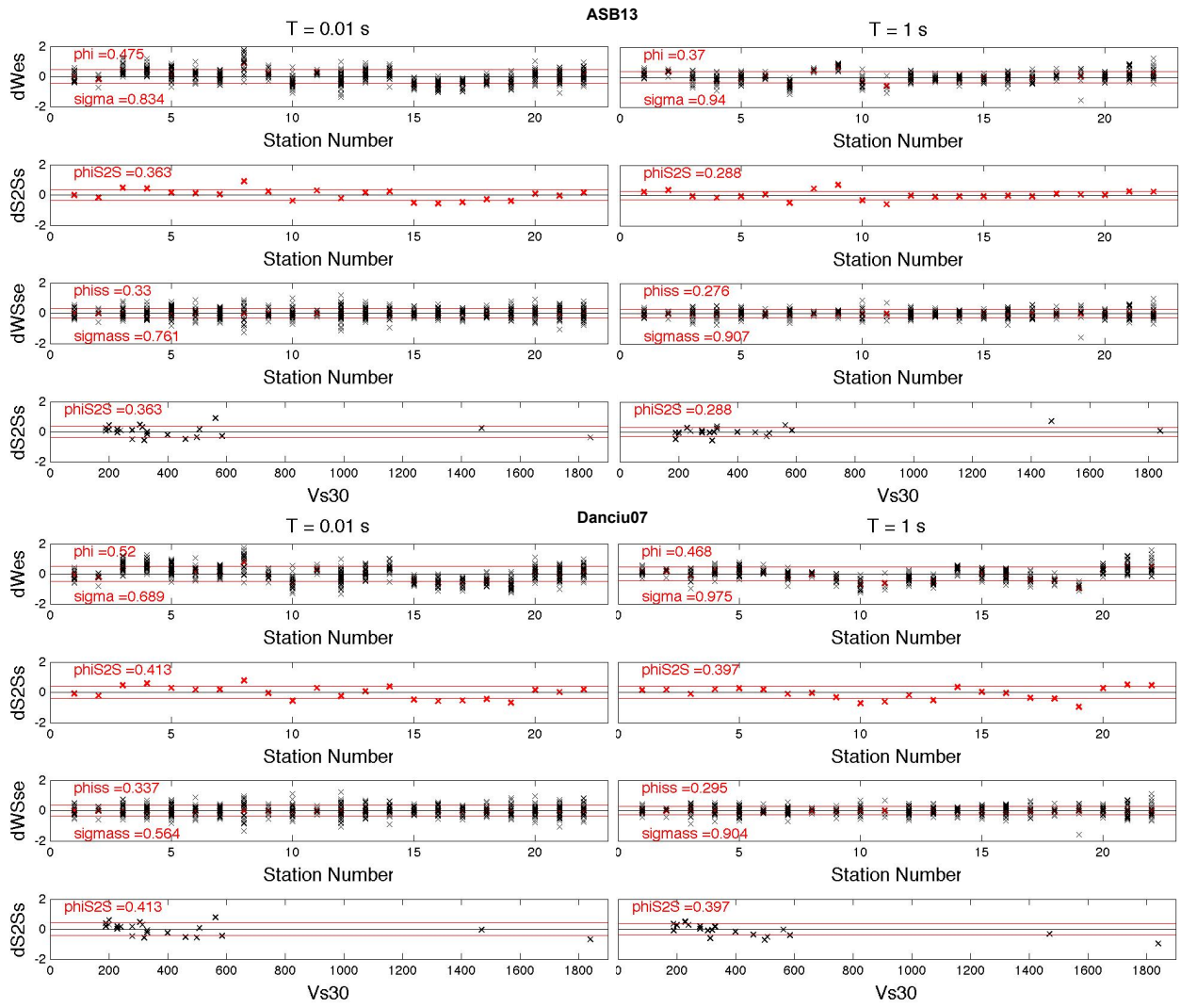

Figure 3.19. Break-up of within-event residuals between observed spectral accelerations at 100 Hz (left) and 1 Hz (right) and the predictions of two GMPEs: Akkar et al. (2014), top, and Danciu and Tselentis (2007), bottom.

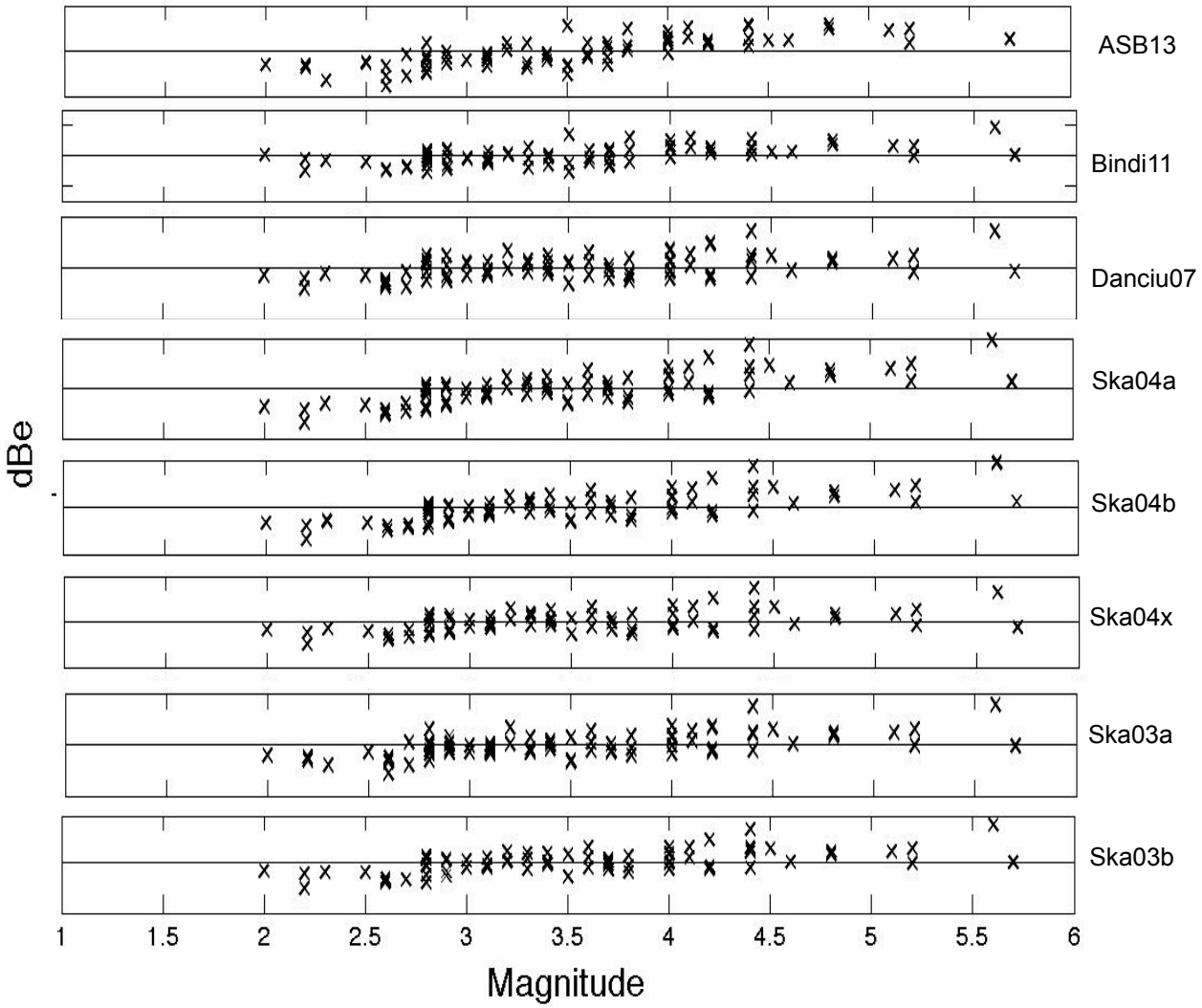

Figure 3.20. Between-event residuals for observed spectral accelerations at 100 Hz for all GMPEs used, showing clear trends with magnitude.

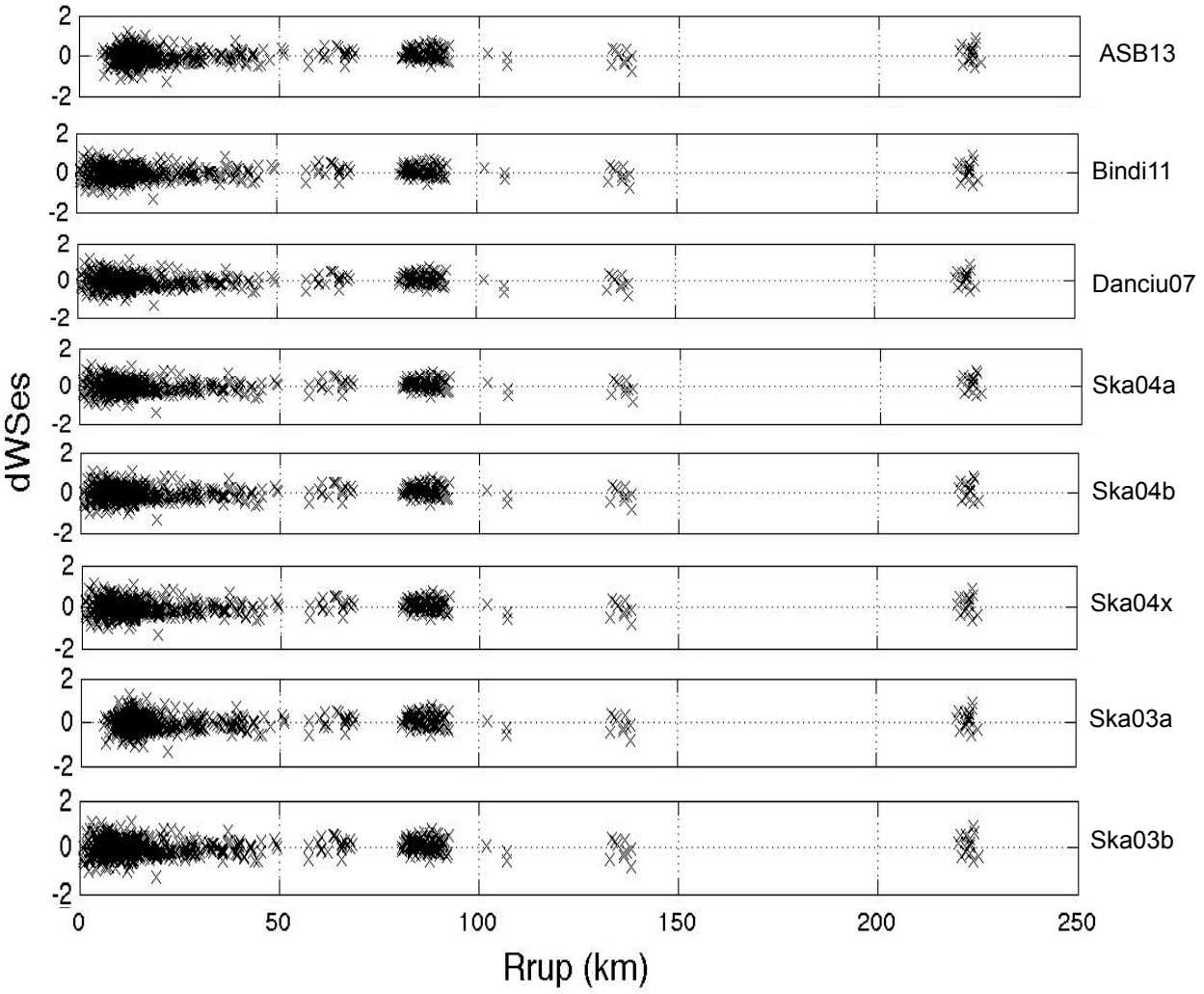

Figure 3.21. Within-event residuals for observed spectral accelerations at 100 Hz for all GMPEs used, showing no discernible trends with distance.

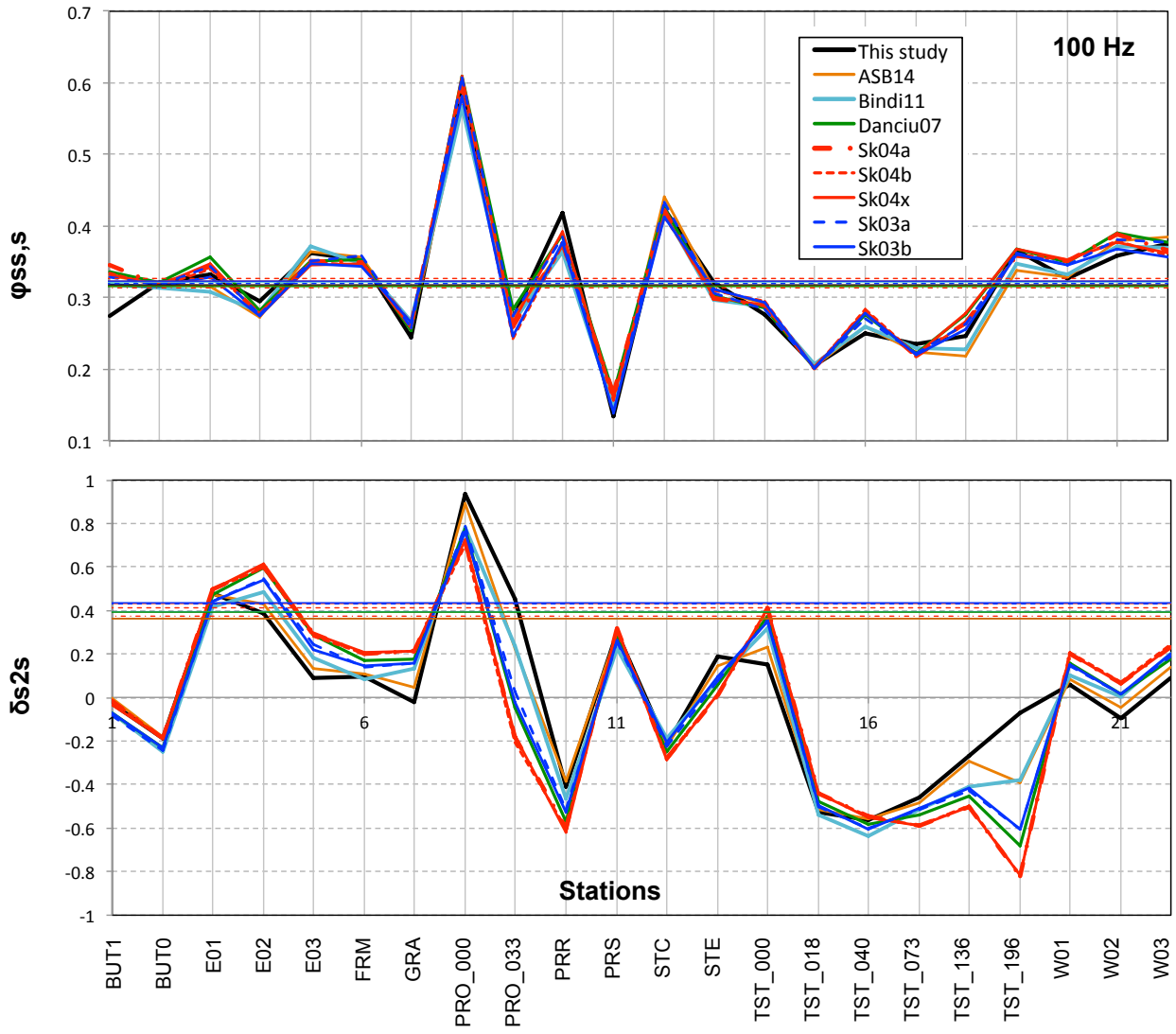

Figure 3.22a. Comparison of the standard deviation components δs2s and φss,s computed for PGA using the following GMPEs: Akkar et al. (2014), Bindi et al. (2011), Danciu and Tselentis (2007), Skarlatoudis et al. (2003), and Skarlatoudis et al. (2004). The standard deviations computed in the first part of this study, fitting a new GMPE to the data, are shown by the black solid line. We note that the overall φss is practically independent of the model used, while φss,s shows some variability for stations E01 and TST_136. φs2s,s shows the largest variability for the two hardest downhole stations: PRO_033 and TST_196.

Figure 3.22b. Same as previous figure, for 1 Hz.

4. COMPARING RECORDED AND SIMULATED VARIABILITY

The reader is referred to Chapter 6 in deliverable SIGMA-2014-D3-137 ('3D ground motion simulations for site effects assessment: learnings from EuroseisTest Verification and Validation Project') listed under WP3, and not available at the time of submission of this document. The chapter deals with preliminary comparisons of ground motion variability between this dataset and the simulations carried out under WP3 and is the product of a collaborative effort between WP2 and WP3.

5. CONCLUSIONS

Our goal is to study ground motion variability in as well constrained a dataset as one may be expected to find today, in terms of records, source parameters, and site information. We optimised our dataset's source parameters (event location and magnitudes) through relocations, catalogue correlations and spectral analysis. We thus managed to significantly reduce the between-event component τ of global aleatory uncertainty σ (by 30% at PGA and up to 50% at 1 Hz). We also achieve a small decrease in τ by implementing quadratic magnitude scaling in our model, despite the small magnitude of our data. The importance of having good site characterisation allows us to decrease φ_{s2s} and hence φ. We compute single-station components of uncertainty and find that, within a partially non-ergodic framework, the total σ can be decreased by about 20% (σ_{ss}) and φ can be decreased by about 30% (φ_{ss}). We compare our single-station values to results found across literature and find them to be lower. They are actually somewhat closer to published single-path estimates. We believe there may be some effect of poor ray coverage in our dataset, but the classic single-path index (the closeness index) does not indicate such effects in our case.

We examine the behaviour of uncertainty components with period from 0.01 to 2 s, and find that τ increases as expected. We find a small peak in the φ_{s2s} around 1.5 Hz, which may indicate greater variability around some of the sites' prevalent resonance frequency. We also investigate the sensitivity of our results to the number of records used. Despite some correlations in the data, we find that a criterion of 3 records per event is sufficient for high frequencies, and is actually necessary to preserve enough data for low frequencies. We next identify the stations of the array with the highest and lowest site variability (φ_{ss}). φ_{ss} does not correlate with Vs30, but we see some possible correlation to 2D/3D wave propagation effects, such as topographic amplification at PRO_000, downgoing wave fields at TST_196, and basin edge effects at PRR, PRS, STC. By binning our data with respect to magnitude, distance and depth, we observe tendencies at different periods. At smaller magnitudes, τ tends to decrease and φ_{ss} tends to increase. This is in agreement with observations made on global datasets for higher event magnitudes. Various reasons can be proposed for this tendency, including poorer constraints and higher stress drop variability for smaller events, which may map on φ_{ss} rather than τ due to kappa and source-site trade-offs. Dependencies with distance and depth can be seen in our data but are less straightforward. The tendency for larger φ_{ss} for small events and distances can also be related to the better ray path coverage the site has for small events, which becomes rather poor for larger events. However, use of Lin's (2011) closeness index does not allow

us to claim single-path effects in this dataset.

Finally, we investigate an alternative approach towards computing φss: the use of existing predictive GMPEs in lieu of creating an ad hoc GMPE with local data. We select some models from Greece and Europe, mostly calibrated for larger magnitudes, but compatible in terms of regional attenuation. All models greatly overpredict ground motion with respect to our data, mainly because of errors in magnitude scaling, which is steeper for our small events. However, we find that the event terms correct for these large errors (the price being much higher τ values) and that within-event residuals are well balanced, which indicates that there is no significant error in distance scaling. Under these two conditions, we find that the φss component can also be computed this way, i.e. by resorting to existing global GMPEs rather than fitting a new one through the data. However, this implies the need to use a regionally applicable model, so that the distance scaling is adequate. We also point out that the GMPE formulation (namely, its site response predictor variable) can affect the systematic deviation δs2s. δs2s can vary between models that account for site response directly through a Vs30 proxy and models that do not account for it, or use site-class-based switches. These differences are large for the two hard rock downhole stations of our array, TST_196 and PRO_33, at all frequencies, especially short ones. However, this does not affect φss,s values overall, which are rather consistent between models at all sites and over all periods.

ACKNOWLEDGEMENTS

Emeline Maufroy, Manu Chaljub, and Pierre-Yves Bard are our collaborators in Chapter 4 (comparison of observed and simulated ground motion variability). Discussions with the experts and members of the SIGMA project and the Next Generation Attenuation (NGA) group are acknowledged, as are discussions with Maria Lancieri, Kyriazis Pitilakis, Dimitris Raptakis, Philippe Renault, Frank Scherbaum. Ezzio Faccioli suggested the idea of testing existing GMPEs. Special thanks to Ronnie Kamai for help on regression issues.

REFERENCES

Akkar, S., Sandikkaya, M.A., Bommer, J.J., 2014b. Empirical ground-motion models for point- and extended-source crustal earthquake scenarios in Europe and the Middle East. Bull. Earthqu. Eng. 12, 359-387.

Al Atik, L., N. Abrahamson, F. Cotton, F. Scherbaum, J. Bommer, and N. Kuehn (2010). The variability of round-motion prediction models and its components, Seismol. Res. Lett. 81: 794–801.

Al Atik L. (2013). Single-Station Phi Using NGA-West2 Data. SSHAC Level 3 Southwestern U.S. Ground Motion Characterization Project, Workshop #2, October 24, Berkeley, CA.

Anderson, J. G., and J. N. Brune (1999). Probabilistic seismic hazard assessment without the ergodic assumption, Seismol. Res. Lett. 70, 19–28.

Anderson, J. G., and Y. Uchiyama (2011). A methodology to improve ground-motion prediction equations by including

path corrections, Bull. Seismol. Soc. Am. 101, 1822–1846.

Atkinson, G. M. (2006). Single-station sigma, Bull. Seism. Soc. Am. 96, 446 – 455.

Bindi D, F. Pacor, L. Luzi, R. Puglia, M. Massa, G. Ameri, R. Paolucci (2011). Ground motion prediction equations derived from the Italian strong motion database. Bull. Earthqu. Eng. 9, 1899-1920.

Boore DM, Atkinson GM (2008) Ground-motion prediction equations for the average horizontal component of PGA, PGV, and 5%-damped PSA at spectral periods between 0.1s and 10.0s. Earthq. Spectra 24, 99-138.

Chen, Y.-H. and C.-C. P. Tsai (2002). A new method for estimation of the attenuation relationship with variance components, Bull. Seism. Soc. Am. 92, 1984 – 1991.

Chen L and E Faccioli (2013). Single-station standard deviation analysis of 2010–2012 strong-motion data from the Canterbury region, New Zealand. Bulletin of Earthquake Engineering 11, 1617−1632.

Chiou, B. S.-J., and R. R. Youngs (2008). An NGA model for the average horizontal component of peak ground motion and response spectra, Earthq. Spectra 24, 173–215.

Danciu, L. and A.-G. Tselentis (2007). Engineering Ground-Motion Parameters Attenuation Relationships for Greece. Bull. Seismol. Soc. Am. 97(1B), 162-183.

Drouet, S., S. Chevrot, F. Cotton, and A. Souriau (2008). Simultaneous inversion of source spectra, attenuation parameters and site responses: application to the data of the French Accelerometric Network, Bull. Seismol. Soc. Am. 98(1), 198-219.

Galanis, O. (2010). Contribution to the development and implementation of algorithms for earthquake location and seismic tomography, PhD Thesis, Aristotle University of Thessaloniki, 320.

Jongmans D., K. Pitilakis, D. Demanet, D. Raptakis, J. Riepl, C. Horrent, K. Lontzetidis and P.-Y. Bard (1998). EURO-SEISTEST: Determination of the geological structure of the Volvi basin and validation of the basin response, Bull. Seism. Soc. Am. 88(2), 473-487.

Klein, F. W. (2002). User's Guide to HYPOINVERSE-2000, a Fortran program to solve for earthquake locations and magnitudes, Open File Report 02-171, U.S. Geological Survey.

Klügel, J.-U., L. Mualchin, and G. F. Panza (2006). A scenario-based procedure for seismic risk analysis, Eng. Geology 88, 1 – 22.

Kudo K., T. Kanno, H. Okada, T. Sasatani, N. Morikawa, P. Apostollidis, K. Pitilakis, D. Raptakis, M. Takahashi, S. Ling, H. Nagumo, K. Irikura, S. Higashi and K. Yoshida (2002). S-Wave Velocity Structure at EURO-SEISTEST, Volvi, Greece Determined by the Spatial Auto-Correlation Method applied for Array Records of Microtremors, Proc. 11th Japan Earthquake Engineering Symposium, Paper No. 62.

Lin, P., N. Abrahamson, M. Walling, C.-T. Lee, B. Chiou, and C. Cheng (2011). Repeatable path effects on the standard deviation for empirical ground-motion models, Bull. Seism. Soc. Am. 101, 2281 – 2295.

Luzi, L., D. Bindi, R. Puglia, F. Pacor, A. Oth (2014). Single-Station Sigma for Italian Strong-Motion Stations. Bull. Seism. Soc. Am. 104(1), 467-483.

Manakou M., D. Raptakis D., F. J. Chavez-Garcia, P. Apostolidis and K. Pitilakis (2010). 3D soil structure of the Mygdonian basin for site response analysis, Soil Dynamics and Earthquake Engineering 30, 1198-1211.

Morikawa, N., T. Kanno, A. Narita, H. Fujiwara, T. Okumura, Y. Fukushima, and A. Guerpinar (2008). Strong motion uncertainty determined from observed records by dense network in Japan, J. Seism. 12, 529 – 546.

Ornthammarath, T, J. Douglas, R. Sigbjörnsson, C.G. Lai (2011). Assessment of ground motion variability and its effects on seismic hazard analysis: a case study for Iceland. Bull. Earthq. Eng. 9, 931-353.

Panagiotopoulos, D.G. (1984), Travel time curves and crustal structure in the southern Balkan region, Ph.D. Thesis, University of Tessaloniki, 159 p. (in Greek).

Pitilakis, K., D. Raptakis, K. Lontzetidis, Th. Tika-Vassilikou & D. Jongmans (1999). Geotechnical & Geophysical

description of EURO-SEISTEST, using field, laboratory tests and moderate strong-motion recordings, J. Earthq. Eng. 3, 381-409.

Pitilakis K., Z. Roumelioti, D. Raptakis, M. Manakou, K. Liakakis, A. Anastasiadis, and D. Pitilakis (2013). The EUROSEISTEST StrongMotion Database and Web Portal, Seismol. Res. Letts 84, 796-804.

Raptakis D., N. Theodulidis and K. Pitilakis (1998). Data Analysis of the EURO-SEISTEST Strong Motion Array in Volvi (Greece): Standard and Horizontal-to-Vertical Spectral Ratio Techniques, Earthquake Spectra 14(1), 203-223.

Raptakis D., F. J. Chávez-García, K. Makra and K. Pitilakis (2000). Site effects at EUROSEISTEST Part I. Determination of the valley structure and confrontation of observations with 1D analysis, Soil Dynamics and Earthquake Engineering 19, 1-22.

Rhoades, D. A. (1997). Estimation of attenuation relations for strong-motion data allowing for individual earthquake magnitude uncertainties, Bull. Seism. Soc. Am. 87(6), 1674 – 1678.

Rodriguez-Marek, A., G.-A. Montalva, F. Cotton, and F. Bonilla (2011). Analysis of single-station standard deviation using the KiK-net data, Bull. Seism. Soc. Am. 101, 1242 – 1258.

Rodriguez-Marek, A., F. Cotton, N. A. Abrahamson, S. Akkar, L. Al Atik, B. Edwards, G. A. Montalva and H. M. Dawood (2013). A model for single-station standard deviation using data from various tectonic regions, Bull. Seism. Soc. Am. 103(6), 3149 – 3163.

Roumelioti, Z., Ch. Benetatos and A. Kiratzi (2010). The instability of the Mw and ML comparison for earthquakes in Greece for the period 1969 to 2007, J. Seism. 14(2), 309 - 337.

Strasser, F., N. A. Abrahamson, and J. J. Bommer (2009). Sigma: Issues, insights, and challenges, Seism. Res. Lett. 80, 40-56, doi: 10.1785/ gssrl.80.1.40.

Skarlatoudis, A. A., C. B. Papazachos, B. N. Margaris, N. Theodoulidis, C. H. Papaioannou, I. Kalogeras, E. M. Scordilis, and V. G. Karakostas (2003). Empirical peak ground motion predictive relations for shallow earthquakes in Greece, Bull. Seismol. Soc. Am. 93, 2591–2603.

Skarlatoudis A., N. theodoulidis, C. Papaioannou, Z. Roumelioti (2004). The dependence of peak horizontal acceleration on magnitude and distance for small magnitude earthquakes in Greece. 13WCEE, Vancouver BC, Canada, 1-6 Aug.